Table III. Adverse events and serious adverse events.

	AE				SAE			
	Placebo (104)		Edaravone (102)		Placebo (104)		Edaravone (102)	
Treatment	*n*	(%)	*n*	(%)	*n*	(%)	*n*	(%)
Total	92	(88.5)	91	(89.2)	24	(23.1)	18	(17.6)
Constipation	17	(16.3)	13	(12.7)				
Dysphagia	12	(11.5)	8	(7.8)	11	(10.6)	8	(7.8)
Nasopharyngitis	22	(21.2)	22	(21.6)				
Muscular weakness	9	(8.7)	7	(6.9)	1	(1.0)	1	(1.0)
Contusion	5	(4.8)	12	(11.8)				
Headache	3	(2.9)	8	(7.8)				
Insomnia	10	(9.6)	9	(8.8)				
Gait disturbance	16	(15.4)	20	(19.6)	2	(1.9)	3	(2.9)
Eczema	2	(1.9)	7	(6.9)				
Glucose urine present	3	(2.9)	6	(5.9)				

All AE with an incidence greater than 5% are tabulated by the primary term, MedDRA version 11.1.

tory disorder and one case of respiratory failure). The investigators determined that the deaths were due to the primary disease and were not related to the study drug. There was no significant inter-group difference in the proportion of SAE ($p = 0.389$). No serious adverse drug reactions occurred in either group.

Discussion

The results of prior clinical trials (20,30) indicated that edaravone may delay the progression of symptoms in some ALS patients. Because evaluation of edaravone would be difficult in patients in whom ALS progression was either acute or non-existent, only patients whose ALSFRS-R score changed by –1 to –4 points during the 12-week pre-observation period were eligible for the study. Since efficacy was found over the 24-week treatment period in the phase II trial, a treatment period of 24 weeks was also chosen for this study.

Based on the results of the previous phase II trial, the inter-group difference in the change of ALSFRS-R score at the end of treatment was expected to be 2 points in this trial. However, the actual inter-group difference was only 0.65 points by ANCOVA and this was not statistically significant. No significant inter-group difference was found by repeated measures analysis of variance either. The results of ANCOVA for pinch strength, a secondary endpoint, suggested a beneficial effect in the edaravone group compared to the placebo group.

Additionally, stratified analysis by diagnostic category (Figure 2) revealed that the change in ALSFRS-R score during treatment was greater in those patients fulfilling the criteria for clinically definite ALS using the Airlie House diagnostic classification. This trial enrolled patients with longer duration of disease and higher ALSFRS-R scores at the start of treatment compared to those of the patients in other trials (31–34). As shown in Table I, the mean duration of disease for the edaravone group and the placebo group was 1.3 years and 1.2 years, respectively, and the mean ALSFRS-R score at the start of treatment was 41 and 42, respectively. While the mean change in ALSFRS-R score during the treatment was –5.70 for the edaravone group and –6.35 for the placebo group, our internal analysis showed that 25% of patients in the edaravone group and 26% of patients in the placebo group showed the change of 0 or –1 point in ALSFRS-R score indicating a more slowly progressive form of the disease than had originally been anticipated when the trial was designed, and thus attenuating the power of the study. Future trials will aim to enroll patients with more rapidly progressive illness. AE occurred in nearly 90% of both groups, i.e. 88.5% of patients in the placebo group and 89.2% in the edaravone group, with no significant differences between the two groups.

In conclusion, although the elimination of free radicals to inhibit the degeneration of motor neurons appears to be a promising new strategy for the treatment of ALS, this study failed to demonstrate efficacy of edaravone to delay the progression of ALS. While the primary endpoint was not achieved, we consider that the results are helpful to identify the patient population in which edaravone could be expected to show efficacy. On the basis of this information, we have designed and are conducting a phase III study.

Acknowledgements

The authors thank all participating patients and their family members, and all the investigators and study coordinators at the 29 centers involved in the trial. Thanks are also due to Mitsubishi Tanabe Pharma Corporation for monitoring of the study, data collection and management, and statistical analysis.

The Edaravone ALS Study Group: Site Investigators

MCI-186 ALS study group investigators are as follows.

Hokkaido University Hospital, Sapporo: Hidenao Sasaki; Hokuyukai Neurological Hospital, Sapporo: Asako Takei, Isao Yamashita; Tohoku University Hospital, Sendai: Masashi Aoki; National Hospital Organization Miyagi National Hospital, Watari: Takashi Imai; Jichi Medical School Hospital, Shimotsuke: Imaharu Nakano; Gunma University Hospital, Maebashi: Koichi Okamoto; Saitama Center of Neurology and Psychiatry, Saitama: Yuichi Maruki; Kohnodai Hospital, National Center for Global Health and Medicine, Ichikawa: Shuichi Mishima, Jin Nishimiya; Toho University Omori Medical Center, Tokyo: Yasuo Iwasaki; Nippon Medical School Hospital, Tokyo: Mineo Yamazaki; The University of Tokyo Hospital, Tokyo: Yuji Takahashi; Kitasato University East Hospital, Sagamihara: Mieko Ogino, Yutaka Ogino; National Center of Neurology and Psychiatry, Kodaira: Masafumi Ogawa; Shonan Fujisawa Tokushukai Hospital, Chigasaki: Tetsumasa Kamei; Seirei Hamamatsu General Hospital, Hamamatsu: Tsuyoshi Uchiyama; Nagoya University Hospital, Nagoya: Hirohisa Watanabe; Mie University Hospital, Tsu: Yasumasa Kokubo; National Hospital Organization Utano Hospital, Kyoto: Hideyuki Sawada; Osaka General Medical Center, Osaka: Takanori Hazama; Osaka Medical College Hospital, Takatsuki: Fumiharu Kimura; National Hospital Organization Toneyama National Hospital, Toyonaka: Harutoshi Fujimura; Kansai Medical University Takii Hospital, Moriguchi: Hirofumi Kusaka; Okayama University Hospital, Okayama: Koji Abe; National Hospital Organization Ehime National Hospital, Toon: Tsukasa Hashimoto; Saiseikai Fukuoka General Hospital, Fukuoka: Takeshi Yamada, Kanamori Yuji, Yamasaki Kenji; Fukuoka Tokushukai Medical Center, Kasuga: Shizuma Kaku; Murakami Karindou Hospital, Fukuoka: Hitoshi Kikuchi; National Hospital Organization Kumamoto Saishunso National Hospital, Koshi: Shigehiro Imamura; National Hospital Organization Miyazaki Higashi Hospital, Miyazaki: Seiichiro Sugimoto, Kishi Masahiko.

Declaration of interest: K. Abe received funding for travel and speaker honoraria from Mitsubishi Tanabe Pharma Corp. Y. Itoyama received speaker honoraria from Mitsubishi Tanabe Pharma Corp. G. Sobue received funding for travel and speaker honoraria from Mitsubishi Tanabe Pharma Corp, and serves on the scientific advisory board for the Kanae Science Foundation for the Promotion of Medical Science, Naito Science Foundation and serves as an advisory board member of Brain, an editorial board member of Degenerative Neurological and Neuromuscular Disease, the Journal of Neurology, and Amyotrophic Lateral Sclerosis and Frontotemporal Degeneration, and received funding from the Ministry of Education, Culture, Sports, Science and Technology of Japan; the Ministry of Welfare, Health and Labor of Japan; the Japan Science and Technology Agency, Core Research for Evolutional Science and Technology. S. Tsuji received funding for travel and speaker honoraria from Mitsubishi Tanabe Pharma Corp. M. Aoki received speaker honoraria, travel expenses, and fees for conducting and consulting on pharmacological test of edaravone in a rat ALS model, from Mitsubishi Tanabe Pharma Corp, and has received research grants, Research on Nervous and Mental Disorders, Research on Measures for Intractable Diseases, Research on Psychiatric and Neurological Diseases and Mental Health from the Japanese Ministry of Health Labor and Welfare, Grants-in-Aid for Scientific Research, an Intramural Research Grant for Neurological Psychiatric Disorders from NCNP and Grants-in-Aid for Scientific Research from the Japanese Ministry of Education, Culture, Sports, Science and Technology. M. Doyu received funding for travel or speaker honoraria from Mitsubishi Tanabe Pharma Corp. C. Hamada is a consultant for Chugai Pharmaceutical Co. Ltd., Taiho Pharmaceutical Co. Ltd., Kowa Company Ltd., Sanwa Kagaku Kenkyusho Co. Ltd., Maruho Co. Ltd., Daiichi Sankyo Co. Ltd., Eisai Co. Ltd., Mochida Pharmaceutical Co. Ltd., Otsuka Pharmaceutical Co. Ltd., Nippon Shinyaku Pharmaceutical Co. Ltd. and Mitsubishi Tanabe Pharma Corp. K. Kondo is an employee of Mitsubishi Tanabe Pharma Corporation. T. Yoneoka is an employee of and co-owns a patent with Mitsubishi Tanabe Pharma Corporation. M. Akimoto is an employee of Mitsubishi Tanabe Pharma Corporation. Y. Yoshino received funding for speaker honoraria from, co-owns a patent with, and is a consultant for Mitsubishi Tanabe Pharma Corp.

The study was funded by Mitsubishi Tanabe Pharma Corporation.

The authors alone are responsible for the content and writing of the paper.

References

1. Rowland LP, Shneider NA. Amyotrophic lateral sclerosis. N Engl J Med. 2001;344:1688–700.
2. Chio A, Logroscino G, Hardiman O, Swingler R, Mitchell D, Beghi E, et al. Prognostic factors in ALS: a critical review. Amyotroph Lateral Scler. 2009;10:310–23.
3. Beckman JS, Carson M, Smith CD, Koppenol W. ALS, SOD and peroxynitrite. Nature. 1993;364:584.
4. Ferrante RJ, Shinobu LA, Schulz JB, Matthews RT, Thomas CE, Kowall NW, et al. Increased 3-nitrotyrosine and oxidative damage in mice with a human Cu/Zn superoxide disumutase mutation. Ann Neurol. 1997;42:326–34.
5. Beal MF, Ferrante RJ, Browne SE, Matthews RT, Kowall NW, Brown RH Jr. Increased 3-nitrotyrosine in both sporadic and familial amyotrophic lateral sclerosis. Ann Neurol. 1997;42:644–54.
6. Abe K, Pan LH, Watanabe M, Kato T, Itoyama Y. Induction of nitrotyrosine-like immunoreactivity in the lower motor

neuron of amyotrophic lateral sclerosis. Neurosci Lett. 1995;199:152–4.
7. Sasaki S, Shibata N, Komori T, Iwara M. iNOS and nitrotyrosine immunoreactivity in amyotrophic lateral sclerosis. Neurosci Lett. 2000;291: 44–8.
8. Tohgi H, Abe T, Yamazaki K, Murata T, Ishizaki E, Isobe C. Remarkable increase in cerebrospinal fluid 3-nitotyrosine in patients with sporadic amyotrophic lateral sclerosis. Ann Neurol. 1999;46:129–31.
9. Itoh K, Wakabayashi N, Katoh Y, Ishii T, Igarashi K, Engel JM, et al. Keap1 represses nuclear activation of antioxidant responsive elements by Nrf2 through binding to the amino-terminal Neh2 domain. Genes Dev. 1999;13:76–86.
10. Arai T, Hasegawa M, Akiyama H, Ikeda K, Nonaka T, Mori H, et al. TDP-43 is a component of ubiquitin-posive tau-negative inclusions in frontotemporal lobar degeneration and amyotrophic lateral sclerosis. Biochem Biophys Res Commun. 2006:351;602–11.
11. Neumann M, Sampathu DM, Kwong LK, Truax AC, Micsenyi MC, Chou TT, et al. Ubiqutinated TDP-43 in frontotemporal lobar degeneration and amyotrophic lateral sclerosis. Science. 2006:314;130–3.
12. Duan W, Li X, Shi J, Guo Y, Li Z, Li C. Mutant TAR DNA-binding protein-43 induces oxidative injury in motor neuron-like cell. Neuroscience. 2010:169;1621–9.
13. The Edaravone Acute Brain Infarction Study Group. Effect of a novel free radical scavenger, edaravone (MCI-186), on acute brain infarction. Cerebravascuar Dis. 2003;15:222–9.
14. Watanabe T, Yuki S, Egawa M, Nishi H. Protective effects of MCI-186 on cerebral ischemia: possible involvement of free radical scavenging and antioxidant actions. J Pharmacol Exp Ther. 1994;268:1597–1604.
15. Mizuno A, Umemura K, Nakashima M. Inhibitory Effect of MCI-186, a free radical scavenger, on cerebral ischemia following the rat middle cerebral artery occlusion. Gen Pharmacol. 1998;30:575–8.
16. Yamamoto T, Yuki S, Watanabe T, Mitsuka M, Saito K, Kogure K. Delayed neuronal death prevented by inhibition of increased hydroxyl radical formation in a transient cerebral ischemia. Brain Research. 1997;762:240–2.
17. Ikeda K, Iwasaki Y, Kinoshita M. Treatment of wobbler mice with free radical scavenger. Molecular Mechanism and Therapeutics of Amyotrophic Lateral Sclerosis. Elsevier Science B.V. 2001;335–40.
18. Ito H, Wate R, Zhang J, Ohnishi S, Kaneko S, Ito H, et al. Treatment with edaravone, initiated at symptom onset, slows motor decline and decreases SOD1 deposition in ALS mice. Exp Neurol. 2008;213:448–55.
19. Aoki M, Warita H, Mizuno H, Suzuki N, Yuki S, Itoyama Y. Feasibility study for functional test battery of SOD transgenic rat (H46R) and evaluation of edaravone, a free radical scavenger. Brain Res. 2011;25:321–5.
20. Yoshino H, Kimura A. Investigation of the therapeutic effects of edaravone, a free radical scavenger, on amyotrophic lateral sclerosis (phase II study). Amyotroph Lateral Scler. 2006; 7:241–5.
21. Brooks BR. Introduction defining optimal management in ALS: from first symptoms to announcement. Neurology. 1999;53:S1–3.
22. Brooks BR, Miller RG, Swash M, Munsat TL. El Escorial revisited: revised criteria for the diagnosis of amyotrophic lateral sclerosis. Amyotroph Lateral Scler Other Motor Neuron Disord. 2000;1:293–9.
23. Cedarbaum JM, Stambler N, Malta E, Fuller C, Hilt D, Thurmond B, et al. The ALSFRS-R: a revised ALS functional rating scale that incorporates assessments of respiratory function. J Neurol Sci. 1999;169:13–21.
24. Ohashi Y, Tashiro K, Itoyama Y, Nakano I, Sobue G, Nakamura S, et al. Study of functional rating scale for amyotrophic lateral sclerosis: revised ALSFRS (ALSFRS-R) Japanese Version. No To Shinkei. 2001;53:346–55. (In Japanese.)
25. Japan intractable diseases information center[online]. Available at: http://www.nanbyou.or.jp/entry/52. Accessed November 13, 2012.
26. Lacomblez L, Bouche P, Bensimon G, Meininger V. A double-blind, placebo-controlled trial of high doses of gangliosides in amyotrophic lateral sclerosis. Neurology. 1989;39:1635–7.
27. Oda E, Ohashi Y, Tashiro K, Mizuno Y, Kowa H, Yanagisawa N. Reliability and factorial structure of a rating scale for amyotrophic lateral sclerosis. No To Shinkei. 1996;48:999–1007. (In Japanese.)
28. Jenkinson C, Fitzpatrick R, Brennen C, Swash M. Evidence for the validity and reliability of the ALS assessment questionnaire: the ALSAQ-40. Amyotroph Lateral Scler Other Motor Neuron Disord. 1999;1:33–40.
29. Yamaguchi T, Ohbu S, Ito Y, Moriwaka F, Tashiro K, Ohashi Y, et al. Validity and clinical applicability of the Japanese version of amyotrophic lateral sclerosis: Assessment questionnaire 40(ALSAQ-40). No To Shinkei. 2004;56: 483–94. (In Japanese.)
30. Yoshino H, Kimura A. Clinical trial for amyotrophic lateral sclerosis with free radical scavenger, edaravone. Neurol Therap. 2003;20:557–64. (In Japanese.)
31. Dupuis L, Dengler R, Heneka MT, Meyer T, Zierz S, Kassubek J, et al. A randomized, double-blind, placebo-controlled trial of pioglitazone in combination with riluzole in amyotrophic lateral sclerosis. PlosOne. 2012;7;6; e37885.
32. Cudkowicz M, Bozik ME, Ingersoll EW, Miller R, Mitsumoto H, Shefner J, et al. The effects of dexpramipexole (KNS-76704) in individuals with amyotrophic lateral sclerosis. Nat Med. 2011;17:1652–6.
33. Pascuzzi RM, Shefner J, Chappell AS, Bjerke JS, Tamura R, Chaudhry V, et al. A phase II trial of talampanel in subjects with amyotrophic lateral sclerosis. Amyotroph Lateral Scler. 2010;11:266–71.
34. Meininger V, Drory VE, Leigh PN, Ludolph A, Robberecht W, Silani V. Glatiramer acetate has no impact on disease progression in ALS at 40 mg/day: a double-blind, randomized, multicentre, placebo-controlled trial. Amyotroph Lateral Scler. 2009;10:378–83.

NEUROPATHOLOGY

Neuropathology 2014; ••, ••–••

doi:10.1111/neup.12105

Case Report

Bunina bodies in motor and non-motor neurons revisited: A pathological study of an ALS patient after long-term survival on a respirator

Tadashi Kimura,[1] Haishan Jiang,[1] Takuya Konno,[2] Makiko Seto,[3] Keisuke Iwanaga,[3] Mitsuhiro Tsujihata,[3] Akira Satoh,[3] Osamu Onodera,[2] Akiyoshi Kakita[1] and Hitoshi Takahashi[1]

Departments of [1]Pathology and [2]Molecular Neuroscience, Brain Research Institute, University of Niigata, Niigata and [3]Section of Neurology, Nagasaki Kita Hospital, Nagasaki, Japan

Bunina bodies (BBs) are small eosinophilic neuronal cytoplasmic inclusions (NCIs) found in the remaining lower motor neurons (LMNs) of patients with sporadic amyotrophic lateral sclerosis (SALS), being a specific feature of the cellular pathology. We examined a case of SALS, unassociated with *TDP-43* or *C9ORF72* mutation, of 12 years duration in a 75-year-old man, who had received artificial respiratory support for 9 years, and showed widespread multisystem degeneration with TDP-43 pathology. Interestingly, in this patient, many NCIs reminiscent of BBs were observed in the oculomotor nucleus, medullary reticular formation and cerebellar dentate nucleus. As BBs in the cerebellar dentate nucleus have not been previously described, we performed ultrastructural and immunohistochemical studies of these NCIs to gain further insight into the nature of BBs. In each region, the ultrastructural features of these NCIs were shown to be identical to those of BBs previously described in LMNs. These three regions and the relatively well preserved sacral anterior horns (S1 and S2) and facial motor nucleus were immunostained with antibodies against cystatin C (CC) and TDP-43. Importantly, it was revealed that BBs exhibiting immunoreactivity for CC were a feature of LMNs, but not of non-motor neurons, and that in the cerebellar dentate nucleus, the ratio of neurons with BBs and TDP-43 inclusions/neurons with BBs was significantly lower than in other regions. These findings suggest that the occurrence of BBs with CC immunoreactivity is intrinsically associated with the particular cellular properties of LMNs, and that the mechanism responsible for the formation of BBs is distinct from that for TDP-43 inclusions.

Key words: amyotrophic lateral sclerosis, Bunina body, cystatin C, non-motor neuron, TDP-43.

INTRODUCTION

Bunina bodies (BBs), which are small eosinophilic neuronal cytoplasmic inclusions (NCIs), are considered to be a specific feature of the cellular pathology in sporadic amyotrophic lateral sclerosis (SALS). BBs are found in lower motor neurons (LMNs) in the spinal cord and brainstem;[1] Piao *et al.* reported that they were observed in 88 (86.3%) of 102 cases of SALS.[2] However, BBs are very rare in the brainstem and in sacral LMNs innervating the striated muscles of the eye and the rectum and urethral sphincter.[1,3,4] Electron microscopy and immunohistochemical studies are important for identifying BBs in patients with SALS: they consist of electron-dense amorphous material often with inner clear areas containing cell organelles, such as filaments (neurofilaments) and vesicles,[1,2] and are immunoreactive for cystatin C (CC), a protein inhibitor of lysosomal cysteine proteases.[1,5]

In SALS, NCIs indistinguishable from BBs may also occur in non-motor neurons,[1] including those in the medullary reticular formation.[6] The ultrastructural features of such NCIs in non-motor neurons have been shown to be identical to those of BBs seen in LMNs.[1,6] However, no reported studies have yet investigated the immunoreactivity of BBs for CC or their relationship to trans-activation response DNA protein 43 (TDP-43) inclusions.

Recently, we encountered a patient with SALS who had survived for a long period on respirator support. In this patient, many small eosinophilic NCIs reminiscent of BBs,

Correspondence: Hitoshi Takahashi, MD, Department of Pathology, Brain Research Institute, University of Niigata, 1-757 Asahimachi, Chuo-ku, Niigata 951-8585, Japan. Email: hitoshi@bri.niigata-u.ac.jp

Received 16 July 2013; revised and accepted 28 December 2013.

which were confirmed in the affected LMNs (described below), were observed in the oculomotor nucleus, medullary reticular formation and cerebellar dentate nucleus. Therefore we performed ultrastructural and immunohistochemical studies of these NCIs to gain further insight into the nature of BBs. Here we describe the clinicopathological features of this patient with new observations on Bunina bodies.

CASE REPORT

The present study was conducted with approval from the Institutional Review Board of the University of Niigata. Written informed consent was obtained from the patient's family prior to these genetic studies of the *TDP-43* and *C9ORF72* genes.

Clinical summary and pathological findings

A 63-year-old man became aware of muscle weakness in the right hand, and over the next 2 years, the muscle weakness extended to all of his extremities. On examination, fasciculation was evident in the tongue and deep tendon reflexes were increased; on this basis he was diagnosed as having ALS. About 3 years after onset, at the age of 66 years, he became bedridden with dysphagia and dyspnea, necessitating tube feeding and artificial respiratory support. Thereafter, ocular movement became limited in all directions, making communication impossible. The patient died of bronchopneumonia at the age of 75 years, about 12 years after disease onset. A general autopsy was performed 3 h after death, at which time the brain weighed 830 g, showing marked frontotemporal atrophy (frontal > temporal) (Fig. 1A).

The brain and spinal cord were fixed in 20% buffered formalin and multiple tissue blocks were embedded in paraffin. Histological examination was performed on 4-μm-thick sections using several stains, including HE, KB and Holzer. Selected sections were also immunostained with antibodies against phosphorylated TDP-43 (pTDP-43) (monoclonal, clone S409/410; Cosmo Bio, Tokyo, Japan; 1:3000, heat/autoclaving) and cystatin C (polyclonal, Dako, Glostrup, Denmark; 1:3000).

The entire spinal cord was markedly atrophic (Fig. 1B) and there was severe wasting in the anterior nerve roots. Histopathological examination revealed that except for the absence of Lewy body-like hyaline inclusions, the entire pathological picture was very similar to that shown in a case of SALS in a 71-year-old woman after long-term survival on a respirator, which we had previously reported.[7] With regard to the motor neuron system, almost complete loss of LMNs was observed in the spinal anterior horns at the levels of the cervical, thoracic and lumbar segments. The sacral anterior horns (S1 and S2), including Onuf's nucleus, contained a number of LMNs (Fig. 1C). In the brainstem, almost complete loss of LMNs was evident in the hypoglossal nucleus. The facial motor nucleus and oculomotor nucleus were relatively well preserved. BBs were found in the remaining LMNs in the sacral anterior horns, including Onuf's nucleus and the facial motor nucleus (Fig. 1D); immunostaining revealed that these BBs were

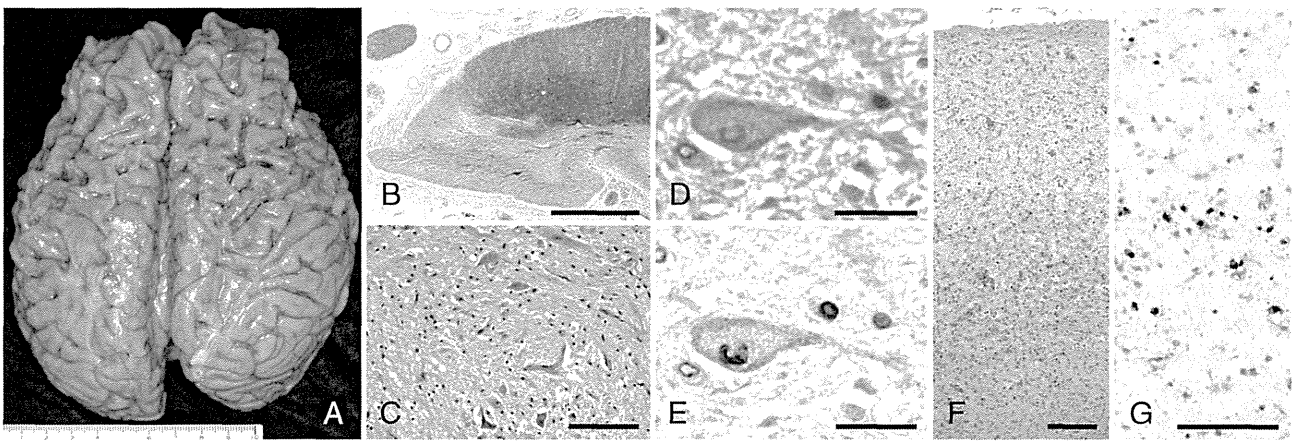

Fig. 1 Neuropathological findings in the brain and spinal cord. Sections stained by the KB method (B), HE (C,D,F) and immunostained with antibodies against cystatin C (CC) (E) and phosphorylated trans-activation response DNA protein 43 (pTDP43) (G). (A) Marked atrophy is evident in the frontal lobe, including the precentral gyrus. (B) The thoracic segment (T2), showing myelin pallor in the white matter except for the posterior columns. (C) Loss of lower motor neurons (LMNs) with gliosis is evident in the sacral (S1) anterior horn. Note that Onuf's nucleus contains a number of LMNs (lower). (D,E) Sequential staining of the same section, showing two facial motor neurons with Bunina bodies (BBs) (D) positive for CC (E). (F) Severe neuronal loss with gliosis is evident in the motor cortex. (G) Here, pTDP-43-positive neuronal cytoplasmic inclusions (NCIs) in layers II-III are shown. Scale bars = 1 mm for (B), 100 μm for (C,G), 20 μm for (D,E) and 200 μm for (F).

positive for CC (Fig. 1E). In the motor cortex, severe neuronal loss was also evident and no Betz cells were found (Fig. 1F); immunostaining revealed pTDP-43-positive NCIs mainly in layers II-III and V-VI (Fig. 1G). The histological findings are summarized in Table 1. Diffuse loss of cerebellar Purkinje cells appeared to be attributable to brain ischemia (Table 1).

Table 1 Pathological findings in the present case

Regions	Loss of neuron	pTDP-43-positive NCIs
Cerebral cortex		
Frontal	+++	+++
Motor	+++	+++
Parietal	++	+++
Cingulate	+++	+++
Insular	+++	+++
Entorhinal	++	+++
Hippocampus (DG/Sub)	+/+++	+++/++
Subcortical area		
Amygdala	++	+++
Basal nucleus of Mynert	+	+
Caudate nuclei	+++/+++	+++/+++
Globus pallidus	+	+++
Thalamus (medial/lateral)	++/+++	++/++
Subthalamic nucleus	nd	nd
Midbrain		
Midbrain tectum	+++	+++
Reticular formation	+++	+++
Oculomotor nucleus	+	+
Red nucleus	+	+
Substance nigra	+++	+
Pons		
Locus celreus	++	+
Reticular formation	++	+++
Facial nucleus (motor)	+	++
Vestibular nucleus	+	+
Pontine nucleus	+	++
Superior olivary nucleus	–	–
Medulla oblongata		
Hypoglossal nucleus	+++	–
Dorsal vagal nucleus	+	++
Reticular formation	++	+++
Nucleus ambiguus	nd	nd
Inferior olivary nucleus	+	+
Cerebellum		
Purkinje cell	+++	–
Granule cell	–	–
Dentate nucleus	+	++
Spinal cord		
Anterior horn	+++	+
Intermediate lateral nucleus	++	++
Clarke's nucleus	+++	–
Posterior horn	++	++
Anterior olfactory nucleus	++	++
Dorsal root ganglia	+	+

Loss of neurons: +, mild; ++, moderate; +++, severe. The numbers of pTDP-43-positive neuronal cytoplasmic inclusions (NCIs) were assessed using a semi-quantitative rating scale: –, absent or nearly absent; +, sparse; ++, moderate; +++, numerous. Hippocampus: DG, dentate gyrus (granule cells); Sub, subiculum. nd, not determined.

TDP-43 mutation and *C9ORF72* repeat expansion analyses

Genomic DNA was prepared from a frozen sample of cerebral cortex from the patient, and then examinations for *TDP-43* mutation and *C9ORF72* repeat expansion were carried out as previously described;[8,9] however, neither of these features was found to be present.

Bunina bodies in motor and non-motor neurons

In addition, the occurrence of many eosinophilic NCIs indistinguishable from BBs in the oculomotor nucleus, medullary reticular formation and cerebellar dentate nucleus was a feature of the present patient. Some representative inclusions in the oculomotor nucleus and medullary reticular formation were recycled for electron microscopy, and small tissue blocks from the formalin-fixed cerebellar dentate nucleus were also processed for ordinary electron microscopy. All of the studied NCIs, 2–3 in each region (Fig. 2A–C), were identified as BBs from their characteristic ultrastructural features (Fig. 2D–F). In the medullary reticular formation, the BB-containing neurons were distributed more widely than previously recorded.[6]

We then investigated the presence or absence of CC immunoreactivity in the BBs, as well as the correlation between the occurrence of BBs and that of pTDP-43-positive inclusions. Four-micrometer-thick paraffin sections that contained the bilateral oculomotor nuclei and medullary reticular formation, and unilateral cerebellar dentate nucleus were prepared, and then stained with HE, observed and photographed (Fig. 3A–C,G–I). They were then destained in absolute ethanol and finally immunostained for CC (Fig. 3D–F) or pTDP-43 (Fig. 3J–L). For comparison, the bilateral sacral anterior horns (S1 and S2) and facial motor nuclei were also similarly examined. The degrees of cytoplasmic staining intensity for CC were generally decreased in the LMNs containing BBs (Fig. 1E,3D–F). pTDP-43-positive NCIs appeared as fine to coarse granular (Fig. 3J), linear wisp-like, large irregular (Fig. 3K) or small round-to-oval inclusions (Fig. 3L); the small round-to-oval inclusions were often observed in neurons in the cerebellar dentate nucleus (Fig. 3L). In each region, the ratio of neurons containing CC-positive BBs to the total cell count of neurons containing BBs was calculated in one section. Similarly, the ratio of neurons containing both BBs and pTDP-43-positive inclusions to the total cell count of neurons containing BBs was calculated in one section. The results obtained are shown in Table 2.

DISCUSSION

Based on the distribution and severity of neuron loss and TDP-43 inclusions, the present case was considered to be

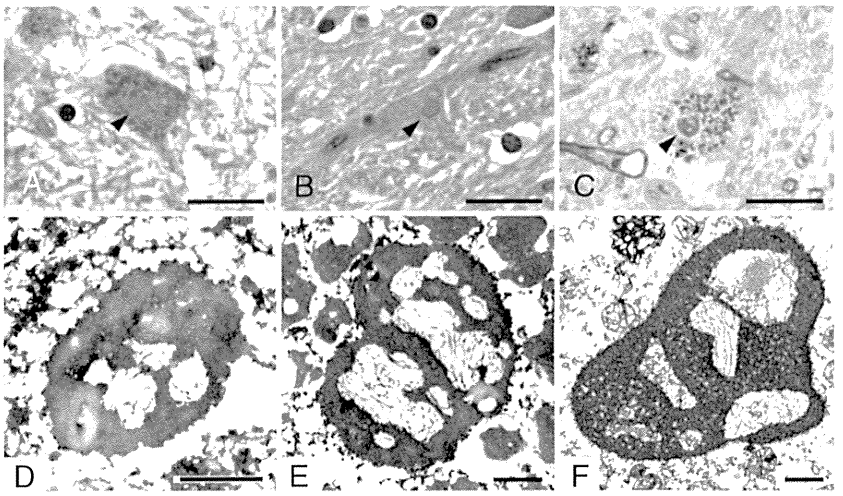

Fig. 2 Ultrastructural profiles of Bunina bodies (BBs) in neurons from the oculomotor nucleus (A), medullary reticular formation (B) and cerebellar dentate nucleus (C). Two paraffin sections stained with HE (A,B) and one Epon section stained with toluidine blue (C). Electron microscopy shows that all the BBs (A–C; arrowheads) have essentially the same ultrastructural profiles, appearing as electron-dense amorphous material with inner clear areas, in which filamentous structures are evident (D–F). In a Bunina body shown in (C), some of the filamentous structures can be identified as neurofilaments, or short fragments of the rough endoplasmic reticulum (F). Scale bars = 20 μm for A–C and 1 μm for D–F.

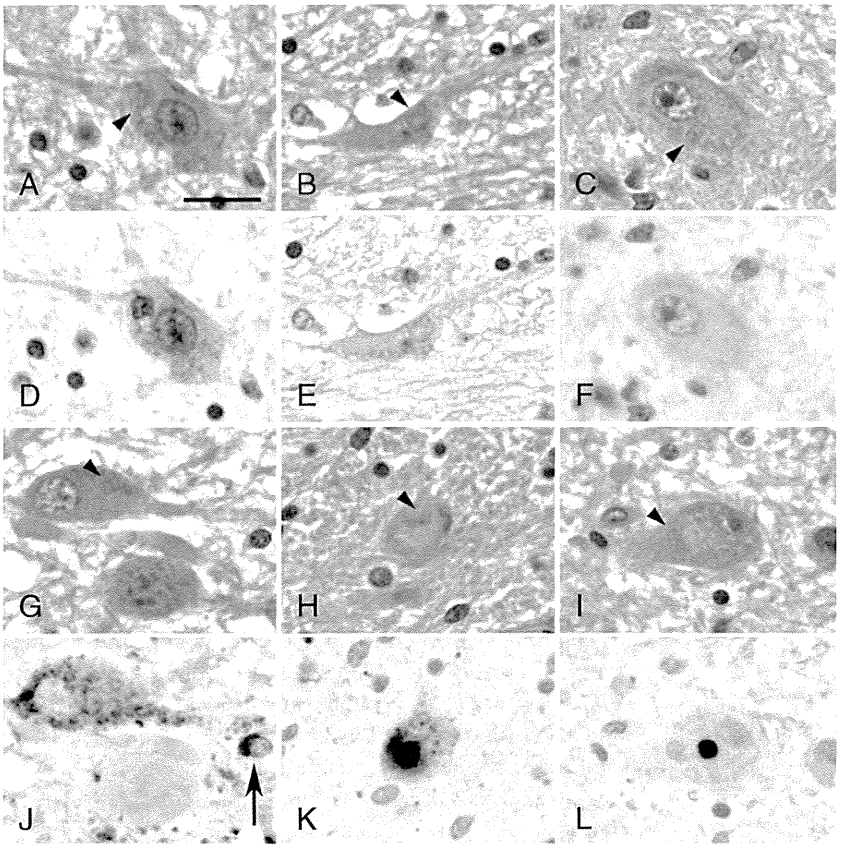

Fig. 3 Immunohistochemical profiles of Bunina bodies (BBs) in neurons from the oculomotor nucleus (A,G), medullary reticular formation (B,H) and cerebellar dentate nucleus (C,I). Sequential staining of the same sections with HE (A–C) and anti-cystatin C (CC) antibody (D–F), as well as with HE (G–I) and anti-phosphorylated trans-activation response DNA protein 43 (pTDP43) antibody (J–L). (A–F) BBs (arrowheads) seen in one lower motor neuron (A) and two non-motor neurons (B,C) are positive (D) and negative (E,F) for CC, respectively. (G–L) In all of the neurons, coexistence of BBs (arrowheads) and pTDP-43-positive neuronal cytoplasmic inclusions (NCIs) is evident; BBs themselves are negative for pTDP-43 (G,J; H,K; I,L). Arrow indicates cytoplasm of a glial cell positive for pTDP-43 (J). Scale bar = 20 μm for (A–L).

an additional example of SALS whose course had been extended by artificial respiratory support, showing widespread multisystem degeneration with TDP-43 pathology (Table 1) (Nishihira *et al.*, Type 2;[10] frontotemporal lobar degeneration – TDP pathology, Type B[11]). We reviewed seven cases in which artificial respiratory support had been used (disease duration, >10 years; Type 1 = 5, Type 2 = 2[10]) and found no NCIs indistinguishable from BBs in the oculomotor nucleus, medullary reticular formation or cerebellar dentate nucleus. In the case (disease duration = $8^2/_3$ years) reported by Nishihira *et al.*,[7] only one BB, which was confirmed by electron microscopy of recycled material, was found in the medullary reticular formation (data not shown). Therefore, the present case, which lacked *TDP-43*

Table 2 Summary of pathological findings for Bunina bodies (BBs)

Region	Ratio (cystatin C)	Ratio (pTDP-43)
Sacral anterior horn	0.88 (7/8)	1.00 (5/5)
Facial motor nucleus	1.00 (8/8)	0.90 (9/10)
Oculomotor nucleus	1.00 (10/10)	1.00 (13/13)
Medullary reticular formation	0.17 (2*/12)†	0.77 (10/13)
Cerebellar dentate nucleus	0.00 (0/36)†	0.33 (12/ /36)††

Ratio (cystatin C): neurons with cystatin C-positive BBs/neurons with BBs; Ratio (pTDP-43): neurons with BBs and pTDP-43-positive inclusions/neurons with BBs. *Regarded as weakly positive. †$P < 0.01$ versus. sacral anterior horn, facial motor nucleus or oculomotor nucleus. ††$P < 0.05$ versus sacral anterior horn, and $P < 0.01$ versus facial motor nucleus, versus oculomotor nucleus or versus medullary reticular formation. Statistical analyses were performed by Ryan's multiple comparison tests using R software (http://www.r-project.org/).

or *C9OLF72* mutation, appeared to be very unusual in terms of the occurrence of BBs even among cases of SALS whose course had been extended by artificial respiratory support.

At present, TDP-43 is widely recognized to be the pathological protein in SALS.[10,12] BBs have been reported to be negative for TDP-43,[12] which was also confirmed in the present study using a monoclonal antibody against pTDP-43. However, the presence of both BBs and TDP-43-positive NCIs has also been shown to be a characteristic feature of ALS with *TDP-43* mutations,[8,12] emphasizing anew the significance of BBs as a specific feature of the cellular pathology of ALS.

Importantly, the present case is the first reported example in which the presence of BBs exhibiting immunoreactivity for CC was a feature of LMNs, but not of non-motor neurons (Table 2). At the ultrastructural level, it is noteworthy that in LMNs, the electron-dense material considered to represent BBs themselves is negative for CC;[5,13] it has been reported that CC immunoreactivity is markedly decreased in the spinal LMNs in SALS, and that the formation of TDP-43 inclusions, but not BBs, may be linked to the CC content of these LMNs.[13] Based on the present findings, we consider that the occurrence of BBs showing CC immunoreactivity is a phenomenon confined almost exclusively to LMNs, and that this must be associated with the particular cellular properties that characterize the LMNs themselves.

The present case is also the first reported to have demonstrated BBs in neurons in the cerebellar dentate nucleus. It has been reported that there is a significant positive correlation between the occurrence of BBs and that of TDP-43 inclusions in spinal and brainstem LMNs.[14,15] This also appears to be the case in the medullary reticular formation (Table 2). However, the ratio (pTDP-43) was significantly lower in the cerebellar dentate nucleus than in other regions (Table 2), indicating that the mechanism responsible for the formation of BBs is distinct from that for TDP-43 inclusions.

Finally, even though the present study involved only a single case and revealed negativity for BBs, as in other similar cases of SALS mentioned above, the results obtained are of considerable interest. In conclusion, the nature and origin of BBs still remain uncertain. When considering why LMNs are generally most vulnerable in ALS, further studies on the formation of BBs in association with the cellular molecular properties of LMNs are needed to elucidate the pathomechanism underlying the disease.

ACKNOWLEDGMENTS

We thank C. Tanda, S. Nigorikawa, J. Takasaki, H. Saito, T. Fujita and S. Egawa for their technical assistance. This work was supported by a Grant-in-Aid, 23240049, for Scientific Research from the Ministry of Education, Culture, Sports, Science and Technology, and a Grant-in-Aid from the Research Committee for CNS Degenerative Diseases, the Ministry of Health, Labour and Welfare, Japan.

REFERENCES

1. Okamoto K, Mizuno Y, Fujita Y. Bunina bodies in amyotrophic lateral sclerosis. *Neuropathology* 2008; **28**: 109–115.
2. Piao YS, Wakabayashi K, Kakita A *et al.* Neuropathology with clinical correlations of sporadic amyotrophic lateral sclerosis: 102 autopsy cases examined between 1962 and 200. *Brain Pathol* 2003; **12**: 10–22.
3. Okamoto K, Hirai S, Amari M, Iizuka T, Watanabe M, Murakami N. Oculomotor nuclear pathology in amyotrophic lateral sclerosis. *Acta Neuropathol* 1993; **85**: 458–462.
4. Okamoto K, Hirai S, Ishiguro K, Kawarabayashi T, Takatama M. Light and electron microscopic and immunohistochemical observations of the Onuf's nucleus of amyotrophic lateral sclerosis. *Acta Neuropathol* 1991; **81**: 610–614.
5. Okamoto K, Hirai S, Amari M, Watanabe M, Sakurai A. Bunina bodies in amyotrophic lateral sclerosis immunostained with rabbit anti-cystatin C serum. *Neurosci Lett* 1993; **162**: 125–128.
6. Nakano I, Iwatsubo T, Hashizume Y, Mizutani T. Bunina bodies in neurons of the medullary reticular formation in amyotrophic lateral sclerosis. *Acta Neuropathol* 1993; **85**: 471–474.
7. Nishihira Y, Tan CF, Toyoshima Y *et al.* Sporadic amyotrophic lateral sclerosis: widespread multisystem degeneration with TDP-43 pathology in a patient after long-term survival on a respirator. *Neuropathology* 2009; **29**: 689–696.

8. Yokoseki A, Shiga A, Tan CF *et al.* TDP-43 mutation in familial amyotrophic lateral sclerosis. *Ann Neurol* 2008; **63**: 538–542.
9. Konno T, Shiga A, Tsujino A *et al.* Japanese amyotrophic lateral sclerosis patients with GGGGCC hexanucleotide repeat expansion in *C9ORF72*. *J Neurol Neurosurg Psychiatry* 2013; **84**: 398–401.
10. Nishihira Y, Tan CF, Onodera O *et al.* Sporadic amyotrophic lateral sclerosis: two pathological patterns shown by analysis of distribution of TDP-43-immunoreactive neuronal and glial cytoplasmic inclusions. *Acta Neuropathol* 2008; **116**: 169–182.
11. Mackenzie IR, Neumann M, Baborie A *et al.* A harmonized classification system for FTLD-TDP pathology. *Acta Neuropathol* 2011; **122**: 111–113.
12. Tan CF, Eguchi H, Tagawa A *et al.* TDP-43 immunoreactivity in neuronal inclusions in familial amyotrophic lateral sclerosis with or without SOD1 gene mutations. *Acta Neuropathol* 2007; **113**: 535–542.
13. Mori F, Tanji K, Miki Y, Wakabayashi K. Decreased cystatin C immunoreactivity in spinal motor neurons and astrocytes in amyotrophic lateral sclerosis. *J Neuropathol Exp Neurol* 2009; **68**: 1200–1206.
14. Mori F, Tanji K, Miki Y, Kakita A, Takahashi H, Wakabayashi K. Relationship between Bunina bodies and TDP-43 inclusions in spinal anterior horn in amyotrophic lateral sclerosis. *Neuropathol Appl Neurobiol* 2010; **36**: 345–352.
15. Mori F, Kakita A, Takahashi H, Wakabayashi K. Co-localization of Bunina bodies and TDP-43 inclusions in lower motor neurons in amyotrophic lateral sclerosis. *Neuropathology* 2013. doi:10.1111/neup.12044

nature COMMUNICATIONS

ARTICLE

Received 25 Feb 2014 | Accepted 16 Apr 2014 | Published 4 Jun 2014

DOI: 10.1038/ncomms4917

The FAM3 superfamily member ILEI ameliorates Alzheimer's disease-like pathology by destabilizing the penultimate amyloid-β precursor

Hiroshi Hasegawa[1,*,†], Lei Liu[1,*], Ikuo Tooyama[1], Shigeo Murayama[2] & Masaki Nishimura[1]

Accumulation of amyloid-β peptide (Aβ) in the brain underlies the pathogenesis of Alzheimer's disease (AD). Aβ is produced by β- and γ-secretase-mediated sequential proteolysis of amyloid-β precursor protein (APP). Here we identify a secretory protein named interleukin-like epithelial-mesenchymal transition inducer (ILEI, also known as FAM3 superfamily member C) as a negative regulator of Aβ production. ILEI destabilizes the β-secretase-cleaved APP carboxy-terminal fragment, the penultimate precursor of Aβ, by binding to the γ-secretase complex and interfering with its chaperone properties. Notch signalling and γ-secretase activity are not affected by ILEI. We also show neuronal expression of ILEI and its induction by transforming growth factor-β signalling. The level of secreted ILEI is markedly decreased in the brains of AD patients. Transgenic (Tg) overexpression of ILEI significantly reduces the brain Aβ burden and ameliorates the memory deficit in AD model mice. ILEI may be a plausible target for the development of disease-modifying therapies.

[1] Molecular Neuroscience Research Center, Shiga University of Medical Science, Seta-Tsukinowa, Otsu, Shiga 520-2192, Japan. [2] Department of Neuropathology, Tokyo Metropolitan Institute of Gerontology, Tokyo 173-0015, Japan. * These authors contributed equally to this work. † Present address: Minami-Kyoto Hospital, Kyoto, Japan. Correspondence and requests for materials should be addressed to M.N. (e-mail: mnishimu@belle.shiga-med.ac.jp).

The amyloid-β peptide (Aβ) is produced in neurons by two-step proteolytic processing of the amyloid-β precursor protein (APP)[1]. Ectodomain shedding by β-secretase, which is known as β-site APP-cleaving enzyme 1 (BACE1), yields the membrane-spanning carboxy-terminal fragment (CTF)-β. The aspartyl protease γ-secretase complex, which primarily comprises presenilin, nicastrin (NCT), anterior pharynx defective-1 (APH-1) and presenilin enhancer-2 (PEN-2), sequentially catalyses intramembrane proteolysis of APP-CTFβ, resulting in secretion of Aβ and liberation of the APP intracellular domain[1]. Each proteolysed derivative exhibits distinct physiological activities[2], and genetic ablation of APP in mice causes neurological deficits such as impairment of spatial learning and reduction in brain weight, which can be completely rescued by expression of the secreted ectodomain[3]. Ablation of the γ-secretase complex by genetic deletion of any of the core components causes early developmental defects that resemble a Notch phenotype, which is expected because γ-secretase is involved in transmembrane signal transduction by cleaving various membrane-spanning substrates, including Notch receptors[1].

A persistent imbalance between production and clearance of Aβ results in gradual accumulation of soluble and aggregated Aβ in the extracellular space of the brain parenchyma, which underlies the development of Alzheimer's disease (AD). Genetic mutations in APP, presenilin-1 (PS1) and presenilin-2 (PS2) modify Aβ biosynthesis and cause an autosomal dominant form of AD[4]. In contrast, alteration in Aβ metabolism in the common sporadic form of AD has not been fully clarified. However, an increase in the amount and activity of BACE1 and/or a decline in protein degradation capacity have been proposed as the primary events in the pathogenesis of sporadic AD[5–8]. In addition to Aβ, accumulation of APP-CTFs, which are sometimes associated with sporadic AD, may cause neurodegeneration by inducing abnormal membrane currents, decreased numbers of dendritic spines, neuronal cell death and inflammatory reactions[9,10].

Reduction in brain Aβ is the pivotal goal of disease-modifying therapy for AD. Although γ-secretase is a major target for therapeutic intervention, non-selective inhibition of its activity causes serious adverse effects due to blockade of Notch signalling and accumulation of neurotoxic APP-CTFs[1,11–13]. To avoid these adverse effects, finding novel approaches to negatively modulate Aβ generation is imperative. Several endogenous proteins interact with the γ-secretase complex and influence the efficacy of γ-secretase cleavage in distinct ways, including alteration of specific activities, substrate selectivity and assembly or subcellular localization of γ-secretase complexes[14–17].

In this study, we searched for additional proteins that affect Aβ generation by interacting with the γ-secretase complex. To date, multiple γ-secretase-modulating proteins have been identified by purification of intact γ-secretase complexes via affinity-mediated isolation of the major catalytic component, PS1 (refs 18,19), which is also involved in cellular Ca homeostasis, apoptosis and protein trafficking by binding additional or alternative partners[14]. In contrast, PEN-2 is exclusively involved in formation of the γ-secretase complex, as the cellular accumulation of PEN-2 is entirely dependent on the expression of the other core components. In addition, PEN-2 is the last component to be incorporated into the γ-secretase complex, and activated complexes exclusively contain PEN-2. Here, using PEN-2 affinity-mediated isolation of the γ-secretase complex, we identify a unique secretory protein that reduces cellular Aβ generation without inhibiting γ-secretase activity or Notch cleavage.

Results

ILEI is a γ-secretase complex-binding protein. We employed tandem affinity-tag purification (TAP)[20] to isolate the γ-secretase complex using PEN-2 as the bait, combined with stable silencing of endogenous PEN-2 expression. The abundance and stoichiometry of γ-secretase components are tightly regulated. Although exogenous PEN-2 can be incorporated into the γ-secretase complex by replacing endogenous PEN-2, high PEN-2 overexpression is required for sufficient replacement. To circumvent this problem, we first prepared PEN-2-knockdown HEK293 cell lines in which small interference RNA (siRNA) for PEN-2 was stably expressed. We chose a PEN-2-knockdown cell line that exhibited the lowest levels of PEN-2 expression and Aβ secretion. We then transfected this cell line with siRNA-resistant PEN-2 (srPEN-2) fused with a TAP tag (TAP-srPEN-2) and selected a cell line, referred to as HEK-TAP-PEN-2, which stably expressed TAP-srPEN-2 at a level equivalent to that of endogenous PEN-2. We confirmed that TAP-srPEN-2 was incorporated into the active γ-secretase complex and restored Aβ secretion (Supplementary Fig. 1).

The activity and composition of γ-secretase complexes are sensitive to several detergents but are only slightly affected by 1% 3-[(3-cholamidopropyl)dimethylammonio]-2-hydroxy-1-propanesulfonic acid (CHAPSO)[21]. We prepared CHAPSO lysates of HEK-TAP-PEN-2 cells and performed sequential isolation of TAP-srPEN-2-associated complexes. To distinguish non-specific binding proteins from proteins of interest, we used TAP-tag-transfected PEN-2-knockdown HEK293 (HEK-TAP-empty) cells as a control. Complexes isolated in two independent trials exhibited a similar pattern of banding on SYPRO- and silver-stained SDS–polyacrylamide gel electrophoresis (SDS–PAGE) gels (Fig. 1a). Proteins in each excised gel piece were digested with trypsin and subjected to liquid chromatography-tandem mass spectrometric analysis followed by a search of the Mascot database. Hits included the four core components and some known binding proteins of the γ-secretase complex. One of the identified peptides matched residues 164–179 of a 27-kDa protein referred to as interleukin-like epithelial-mesenchymal transition inducer (ILEI) or family with sequence similarity 3, member C (FAM3C) (NCBI Protein Database accession code NP_055703).

ILEI, which was originally identified in a database search for four-helix-bundle cytokines, is an evolutionarily conserved secretory protein[22]. ILEI is posttranslationally liberated from the membrane in secretory vesicles by cleavage of the signal sequence of the full-length (FL) precursor protein. Immunoblotting with an affinity-purified rabbit polyclonal anti-ILEI antibody revealed specific bands of 24 and 27 kDa in the conditioned medium and cell lysate of HEK293 cells, respectively, suggesting that the smaller species corresponded to a processed, secreted form of ILEI (Fig. 1b). Co-immunoprecipitation using native HEK293 cells indicated that antibodies against PS1, NCT, PEN-2 or APH-1 co-precipitated the precursor and processed forms of ILEI (Fig. 1b). The reverse assay revealed that the anti-ILEI antibody co-precipitated the four core components of the γ-secretase complex (Fig. 1c). Protein complex analysis using two-dimensional Blue Native SDS–PAGE suggested that ILEI is incorporated into multiple complexes of various molecular masses, one of which is comparable to that of the mature γ-secretase complex (Fig. 1d). These data confirmed the interaction between ILEI and the γ-secretase complex.

To determine the partner that directly interacts with endogenous ILEI, we treated HEK293 cells *in situ* with a thiol-cleavable, membrane-permeable, chemical crosslinker. The cells were then lysed in a Nonidet P-40 buffer to dissociate non-crosslinked components of the γ-secretase complex. In this lysate, monomeric components of the γ-secretase complex were reduced

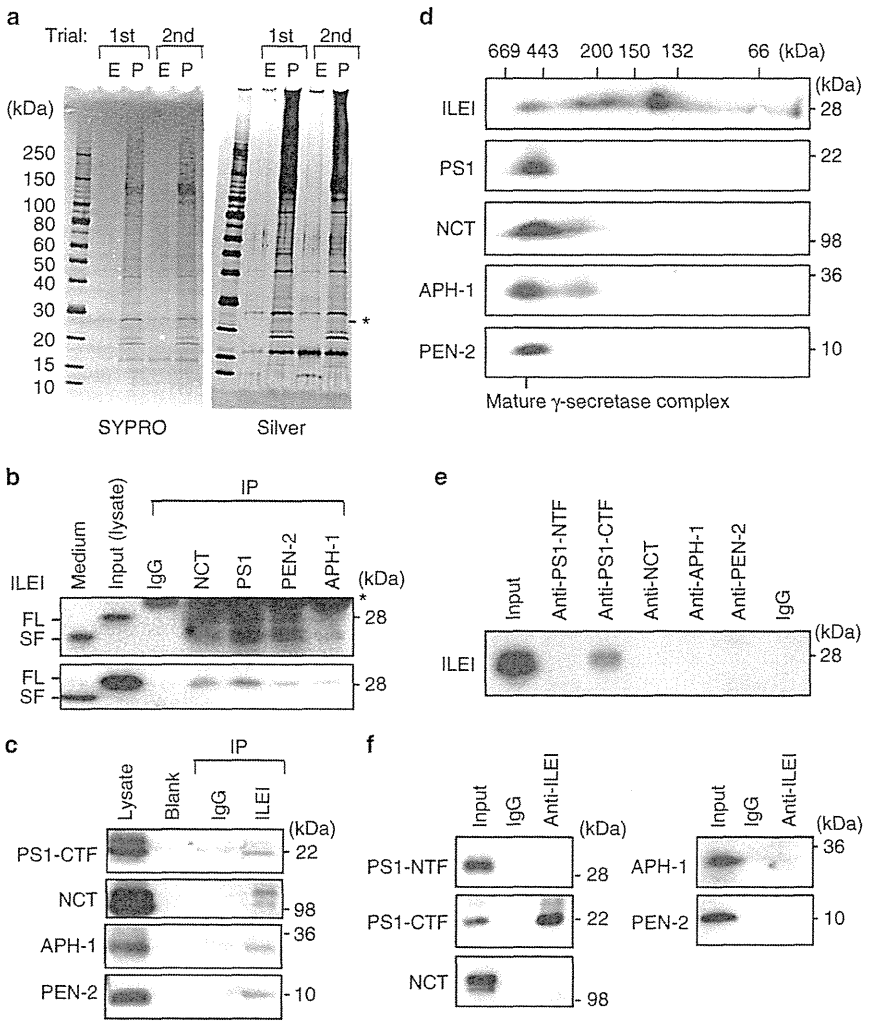

Figure 1 | ILEI is associated with mature γ-secretase complexes. (**a**) SYPRO- and silver-stained SDS-PAGE gels of TAP-tagged PEN-2-associated proteins isolated from lysates of HEK-TAP-PEN-2 (P) and HEK-TAP-empty (E) cells. ILEI was identified in the band indicated by the star. (**b**) Co-immunoprecipitation of endogenous ILEI and γ-secretase components. Native HEK293 cell lysates were immunoprecipitated with normal IgG or an antibody against NCT, PS1, PEN-2 or APH-1. The blot was probed with anti-ILEI antibody (upper panel). As the FL ILEI bands were close to the IgG light-chain bands, nanocapsules incorporating IgG Fc-binding Z domains were used instead of the secondary antibody for detection (lower panel). The star indicates the IgG band. FL, full-length; SF, secreted form. (**c**) Reverse co-immunoprecipitation. HEK293 cell lysates were precipitated using normal rabbit IgG (IP-IgG) or anti-ILEI antibody (IP-ILEI). The blots were probed using the indicated antibodies. (**d**) Two-dimensional Blue Native (BN)/SDS-PAGE analysis of ILEI and γ-secretase components. The membrane fraction of native HEK293 cells was subjected to two-dimensional BN/SDS-PAGE before immunoblotting. (**e**) Chemical crosslinking of ILEI with γ-secretase components. HEK293 cells were crosslinked *in situ* with dithiobis succinimidyl propionate. The 1% Nonidet P-40-solubilized cell lysate was subjected to immunoprecipitation. A blot of the immunoprecipitates with antibodies against the indicated proteins or normal IgG was probed with anti-ILEI antibody. (**f**) The crosslinked cell lysates were immunoprecipitated using normal IgG or anti-ILEI antibody. The blots were probed using the indicated antibodies.

by >80% on immunoblotting. PS1-CTF but not the other components co-immunoprecipitated ILEI (Fig. 1e). Conversely, the ILEI immunoprecipitates contained PS1-CTF but the other components were not present or were only faintly observed (Fig. 1f). These results suggest that ILEI directly binds to PS1-CTF.

ILEI reduces Aβ generation by destabilizing APP-CTFβ. RNA interference (RNAi)-mediated knockdown of endogenous ILEI in native HEK293 cells resulted in an approximately two-fold increase in Aβ40 and Aβ42 levels in the conditioned medium (Fig. 2a). Conversely, overexpression of ILEI decreased Aβ secretion (Fig. 2b). No significant alteration in the ratio of Aβ40 to Aβ42 was observed. ILEI knockdown or overexpression also increased or decreased APP intracellular domain generation, respectively (Fig. 2c).

We next determined whether ILEI affects γ-secretase cleavage of the Notch-1 receptor. Treatment with EDTA enhances the site-2 cleavage of transmembrane/intracellular Notch to generate Notch extracellular truncation, which is then directly cleaved by γ-secretase to release Notch intracellular domain[23]. ILEI

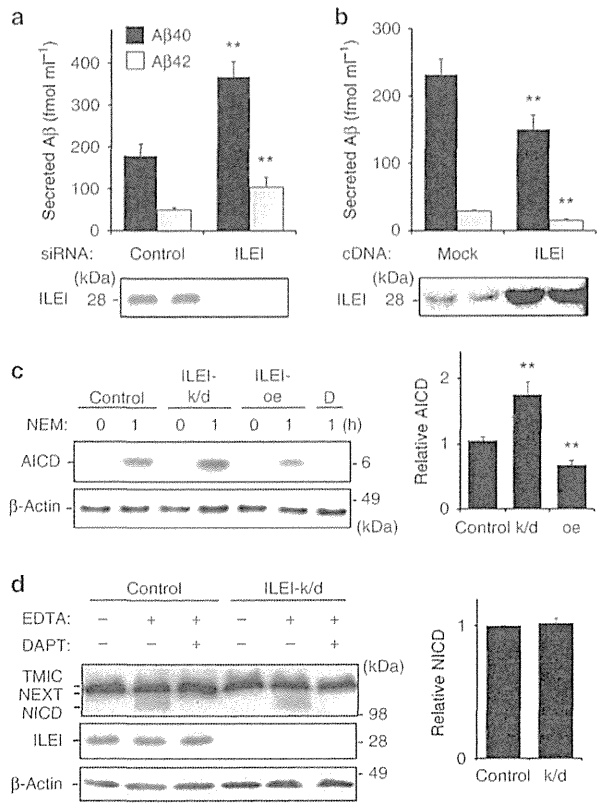

Figure 2 | ILEI inhibits cellular γ-secretase cleavage of APP but not Notch. Non-targeting control or ILEI-specific siRNA (**a**), or mock or ILEI cDNA (**b**) was transiently transfected into HEK293 cells. Aβ40 (black bars) and Aβ42 (grey bars) in the conditioned medium were measured using ELISA assays ($n = 6$, mean ± s.d.). $^{**}P < 0.01$ versus the control or the mock by Student's *t*-test. Lower panels show immunoblots of ILEI. (**c**) Immunoblot for APP intracellular domain (AICD) in control, ILEI-knockdown (k/d) or ILEI-overexpressing (oe) HEK293 cells. Cells were treated with 200 μM *N*-ethylmaleimide (NEM) for 1 h to block degradation of AICD[60]. AICD production was inhibited by DAPT (*N*-[*N*-(3,5-difluorophenacetyl)-L-alanyl]-*S*-phenylglycine *t*-butyl ester; 1 μM) treatment (**d**). The graph shows the relative intensity of AICD normalized to β-actin ($n = 3$, mean ± s.d.). $^{**}P < 0.01$ versus the control by Student's *t*-test. (**d**) Proteolysed derivatives of endogenous Notch-1 in control and ILEI-knockdown (k/d) mouse embryonic fibroblasts (MEFs). EDTA (1.5 mM) treatment induced cleavage of transmembrane/intracellular Notch (TMIC) to generate Notch extracellular truncation (NEXT), which was then cleaved by γ-secretase to release Notch intracellular domain (NICD). NICD production was inhibited by DAPT (1 μM) treatment. The graph shows the relative intensity of NICD normalized to β-actin ($n = 3$, mean ± s.d.). No significant difference versus the control was found ($P > 0.05$ by Student's *t*-test).

knockdown in mouse embryonic fibroblasts did not alter Notch intracellular domain generation from endogenous Notch in the presence of EDTA (Fig. 2d). In addition, we used a cell-based luciferase reporter assay for γ-secretase cleavage of Notch. The specificity was confirmed by treatment with a potent γ-secretase inhibitor, DAPT (*N*-[*N*-(3,5-difluorophenacetyl)-L-alanyl]-*S*-phenylglycine *t*-butyl ester), which attenuated luminescence (35.9 ± 4.5% of vehicle; vehicle, 100.0 ± 6.5%; $n = 5$, $P = 0.000$). Induction of luciferase activity was unaffected by transfection with ILEI siRNA (94.5 ± 12.5% of control; control, 100.0 ± 5.7%; $n = 5$, $P = 0.449$) or ILEI complementary DNA (96.8 ± 8.9% of mock; mock, 100.0 ± 8.2%; $n = 5$, $P = 0.596$). Thus, ILEI does not perturb γ-secretase processing of Notch.

To test whether ILEI directly inhibits γ-secretase activity, we evaluated Aβ generation in a cell-free assay in which microsome fractions derived from HEK293 cells treated with non-targeting control or ILEI-specific siRNA were incubated with excess recombinant APP-CTFβ. Unexpectedly, we found no significant difference in Aβ generation ($n = 6$, $P = 0.851$ for Aβ40; $P = 0.561$ for Aβ42) between control (Aβ40: 3,253.3 ± 399.0, Aβ42: 597.7 ± 23.8 fmol ml^{-1}) and ILEI-knockdown cells (Aβ40: 3,181.9 ± 306.4, Aβ42: 614.5 ± 28.9 fmol ml^{-1}), indicating that ILEI reduces cellular Aβ generation without inhibiting γ-secretase activity. This result and the observation that ILEI was processed normally in the presence of DAPT (Supplementary Fig. 2a) further suggest that ILEI is not a competitive substrate of γ-secretase. In addition, ILEI knockdown did not detectably affect the cellular expression levels or subcellular localization of γ-secretase components, the intracellular trafficking of APP, or the Aβ secretion process (Supplementary Figs 2b-d and 3a). We also excluded the possibility that ILEI accelerated degradation of secreted Aβ in the culture medium (Supplementary Fig. 3b).

Accordingly, ILEI knockdown increased the level of cellular APP-CTFs (APP-CTFα and APP-CTFβ) without augmenting APP-FL or secreted ectodomains of APP (Fig. 3a). ILEI knockdown did not change APP transcript expression as measured with quantitative real-time PCR (104.1 ± 3.8% of control; control, 100.0 ± 2.9%; $n = 3$, $P = 0.291$) or cellular β-secretase activity as measured with an *in vitro* assay (104.4 ± 7.31% of control; control, 100.0 ± 6.1%; $n = 3$, $P = 0.555$). We thus reasoned that ILEI knockdown stabilizes APP-CTFβ to increase Aβ generation. A cycloheximide chase assay indicated that ILEI knockdown significantly extended the half-life of APP-CTFs but not APP-FL (Fig. 3b). Altered ILEI expression levels did not change the levels of Beclin-1 or Rab5a or the subcellular localization of APP-CTFs (Supplementary Fig. 3a and c), suggesting that stabilization of APP-CTFs is not mediated by inactivation of general protein degradation through lysosomal/autophagosomal pathways or a defect in APP-CTF trafficking. The effect of ILEI knockdown on APP metabolism could be rescued by transfection of siRNA-resistant ILEI cDNA (Fig. 3c), ruling out potential off-target effects of the siRNA-mediated RNAi.

We examined whether ILEI also acts on low-density lipoprotein receptor-related protein 1 (LRP1) and N-cadherin, which are other substrates of γ-secretase. Knockdown or overexpression of ILEI did not affect accumulated levels of LRP1 or N-cadherin CTFs (Fig. 3d). Taken together with the results for Notch-1 (Fig. 2d), our results suggest that ILEI exhibits selectivity for APP-CTFs.

ILEI interferes with the APP-CTF-stabilizing property of PS1. Processed ILEI is secreted from the cell, whereas intracellular ILEI is mostly associated with the microsome fraction (Supplementary Fig. 4a). Hence, we next determined whether extracellular application of a secreted form of ILEI decreased cellular Aβ secretion. We purified a recombinant polypeptide of processed ILEI from the conditioned medium of C-terminally V5-His-tagged ILEI (ILEI-VH)-overexpressing HEK293 cells (Supplementary Fig. 4b). When added into the culture medium of ILEI-knockdown HEK293 cells, purified ILEI-VH suppressed the levels of secreted Aβ and cellular APP-CTFs in a dose-dependent manner (Fig. 4a). Purified ILEI-VH was detected in perinuclear vesicular compartments and was associated with PS1 (Fig. 4b,c). These results suggest that ILEI acts on the extracellular side of the cell membrane and is endocytosed into the cell. In contrast, when we added purified ILEI-VH to cell-free mixtures and performed

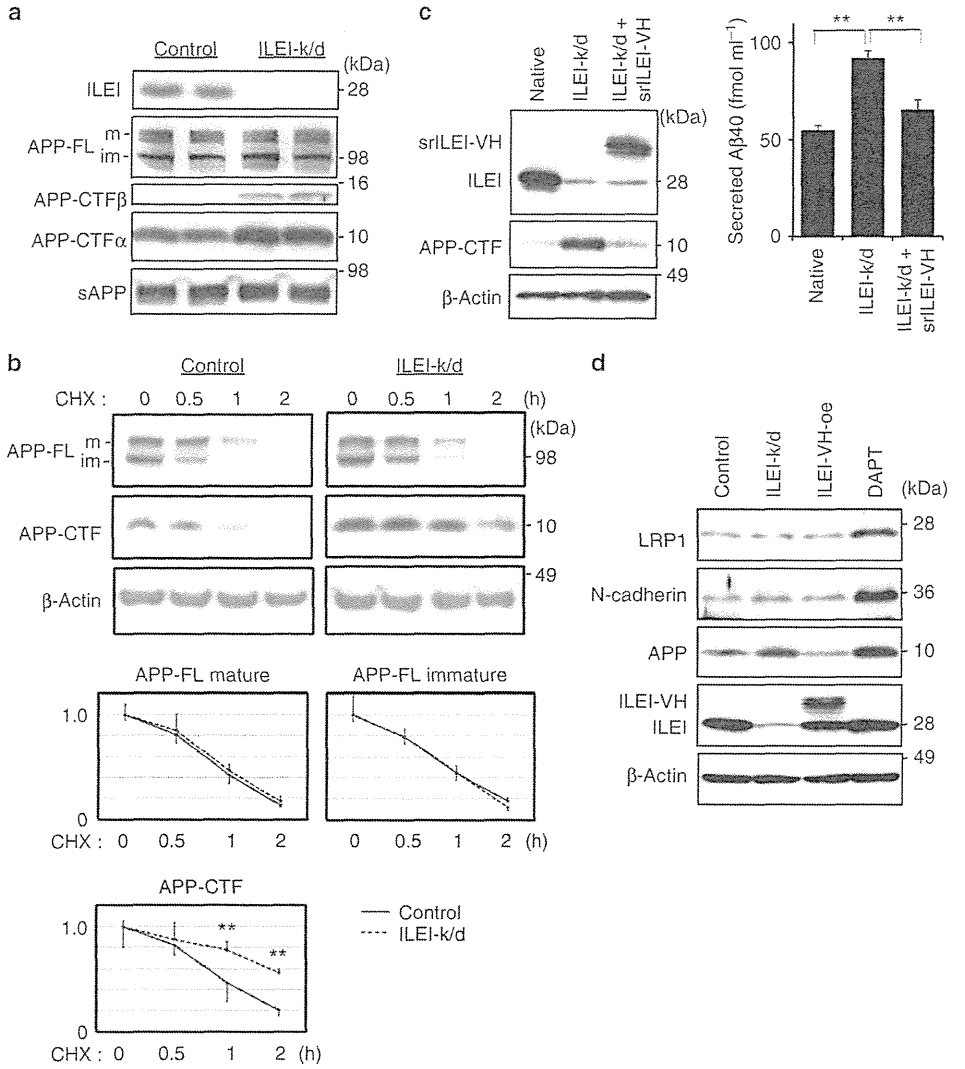

Figure 3 | ILEI knockdown selectively stabilizes APP-CTFs. (**a**) Immunoblots for APP and its proteolysed derivatives in control and ILEI-knockdown (k/d) HEK293 cells. The same amount of protein from cell lysates (for ILEI, APP FL and APP-CTFs) or conditioned medium (for secreted ectodomain; sAPP) was loaded. For APP-CTFβ, a longer exposure image is shown. m, mature; im, immature. (**b**) Immunoblots of APP-FL and APP-CTF in a cycloheximide (CHX) chase assay. m, mature; im, immature. Non-targeting control or ILEI-specific siRNA-transfected HEK293 cells were treated with 50 μg ml^{-1} CHX for the indicated times. β-Actin was used as a loading control. The graphs below show the relative intensity of the bands ($n = 5$, mean ± s.d.). $^{**}P < 0.01$ versus the control by Student's *t*-test. (**c**) The restoring effect of siRNA-resistant ILEI-V5-His (srILEI-VH) on the levels of APP-CTFs and secreted Aβ. ILEI-specific siRNA-transfected HEK293 cells were further transfected with srILEI-VH. APP-CTF was analysed with immunoblotting, and secreted Aβ40 was measured with ELISA ($n = 3$, mean ± s.d.). $^{**}P < 0.01$ by Student's *t*-test. (**d**) Immunoblots for LRP1-CTF (25 kDa), N-cadherin-CTF (36 kDa) and APP-CTF (10 kDa) in control, stable ILEI-knockdown (k/d), stable ILEI-VH-overexpressing (oe) and DAPT (*N*-[*N*-(3,5-difluorophenacetyl)-L-alanyl]-*S*-phenylglycine *t*-butyl ester; 1 μM)-treated HEK293 cells. β-Actin was used as a loading control.

γ-secretase assays using microsome fractions derived from ILEI-knockdown HEK293 cells, Aβ generation was not altered (Supplementary Fig. 4c).

Although we identified ILEI as a γ-secretase complex-binding protein, whether ILEI interaction with the γ-secretase complex mediated the stabilization of APP-CTFs was not clear. To address this issue, we tested the effect of ILEI knockdown on APP-CTF levels in PS1/PS2-knockdown HEK293 cells. High levels of APP-CTFs accumulated in PS1/PS2-knockdown cells in which the γ-secretase complex was ablated. ILEI knockdown did not lead to any further increase in APP-CTFs (Fig. 4d). In contrast, as shown in Fig. 4d, the APP-CTF level was increased by ILEI knockdown in PEN-2-knockdown HEK293 cells, which exclusively contained immature, inactive γ-secretase complexes[24]. Furthermore, ILEI knockdown and ILEI-VH treatment enhanced and reduced accumulation of APP-CTFs in the presence of a γ-secretase inhibitor, respectively (Fig. 4a,d). Thus, ILEI requires interaction with the γ-secretase complex, regardless of whether the complex is enzymatically active or inactive, to alter the stability of APP-CTFs. In contrast, co-immunoprecipitation assays revealed no direct interaction between ILEI and APP-CTFs (Supplementary Fig. 3d).

We next asked whether ILEI competes with APP-CTFs for binding with the γ-secretase complex. Co-immunoprecipitation

assays indicated that the amount of PS1-bound APP-CTFs was inversely correlated with the ILEI expression level (Fig. 4e). In contrast, alternative co-immunoprecipitation assays suggested that the expression level of APP did not influence the amount of PS1-bound ILEI (Fig. 4f). These results imply that ILEI non-competitively interferes with the binding between the γ-secretase complex and APP-CTFs.

The PS1/γ-secretase complex stably binds APP-CTFs and protects them from non-specific degradation[21,25]. Analysis of the APP-CTF-stabilizing property is hampered by γ-secretase

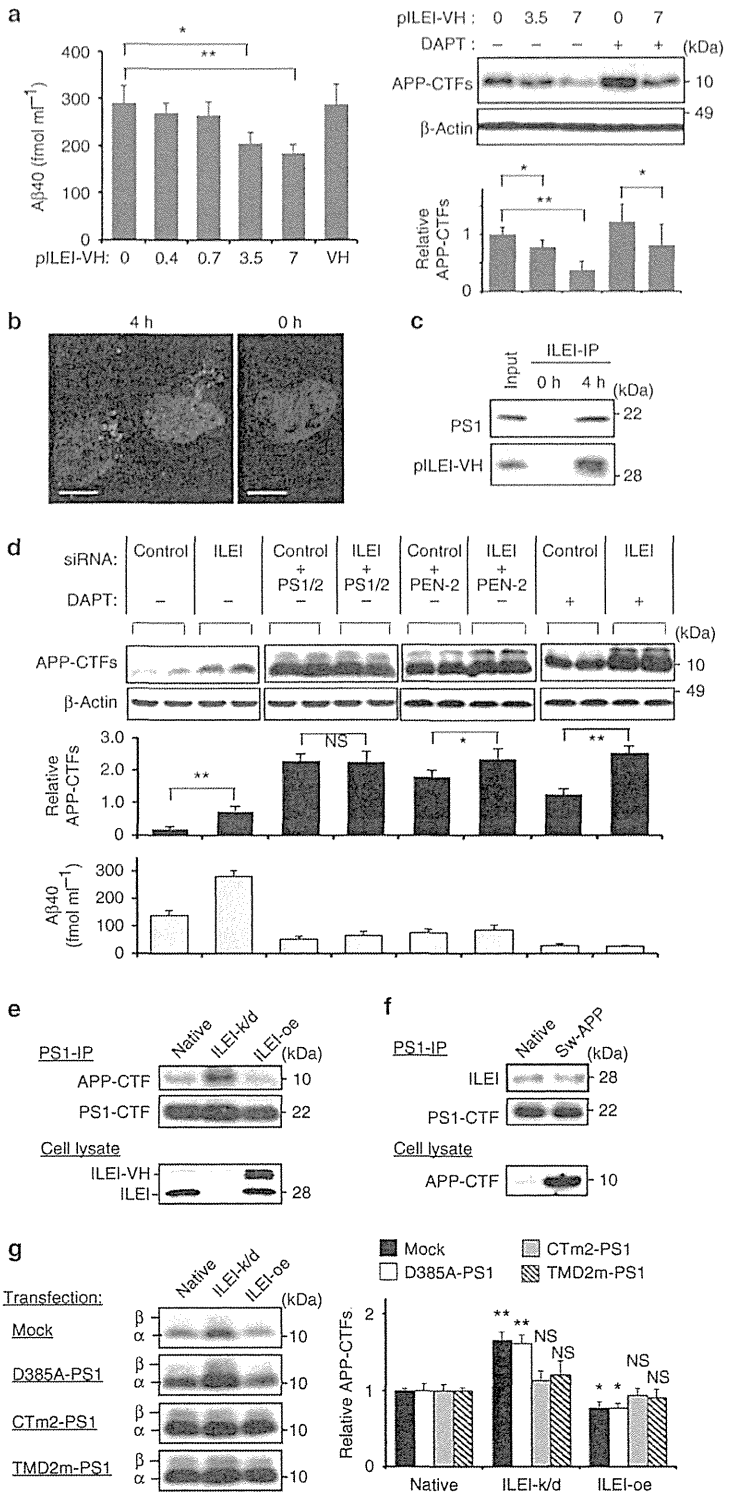

activity, although the former is independent of the latter[25]. To determine whether ILEI interferes with this property, we used three catalytically inactive PS1 mutants: D385A-PS1, CTm2-PS1 and TMD2m-PS1. D385A-PS1 has an alanine substitution of the aspartic acid residue (D^{385}) at the active centre and binds with APP-CTFs and ILEI (Supplementary Fig. 5a–c). CTm2-PS1 has alanine substitutions of D^{385} and the sequential three amino acid residues (D^{458}, Q^{459} and L^{460}) in the extracellular/luminal C-terminal tail and lacks the ability to bind ILEI (Supplementary Fig. 5a,b). TMD2m-PS1, the second transmembrane domain (TMD) of which is replaced with the TMD of CD4 (ref. 26), lacks the ability to bind APP-CTFs (Supplementary Fig. 5c). Overexpression of D385A-PS1 or CTm2-PS1 but not TMD2m-PS1 increased APP-CTFs in PS1/PS2-double knockout mouse embryonic fibroblasts[27] (Supplementary Fig. 5d), suggesting that APP-CTFs are stabilized by the binding with PS1. The APP-CTF-destabilizing effect of ILEI was abrogated by overexpression of CTm2-PS1 or TMD2m-PS1 (Fig. 4g), suggesting that both mutants prevented ILEI from destabilizing APP-CTFs in a dominant-negative manner. Exogenous CTm2-PS1 and TMD2m-PS1 are expected to compete with endogenous PS1 for binding to APP-CTFs and ILEI, respectively. Our results thus imply that APP-CTF destabilization by ILEI requires the interaction between ILEI and PS1, and between PS1 and APP-CTFs. APP-CTFs that accumulated with ILEI knockdown were indeed colocalized with PS1 in subcellular fractions of cultured cells (Supplementary Fig. 3a). These results support our hypothesis that ILEI binds to the PS1/γ-secretase complex and interferes with its APP-CTF-stabilizing property to reduce Aβ generation.

Neuronal expression of ILEI. Previous studies showed that ILEI is expressed in the central nervous system as well as in secretory epithelia[22,28]. However, the regional and cellular distribution of ILEI in mammalian brains has not been examined. We confirmed the specificity of rabbit anti-ILEI antibody (Supplementary Fig. 6) and performed immunohistochemical staining for ILEI. ILEI was widely expressed in mouse and human brains, and was prominent in pyramidal neurons in the cerebral cortex and hippocampus. ILEI-immunoreactive structures were detected in perinuclear regions of neuronal cell bodies, whereas glial fibrillary acidic protein-positive astrocytes and Iba1-positive microglia were negative for ILEI (Fig. 5a). Perinuclear ILEI was colocalized with TGN46, Rab5a and Rab7, indicating that ILEI principally resides in the *trans*-Golgi network and the endocytic vesicles where Aβ is reportedly produced[29,30] (Supplementary Fig. 7). Colocalization of ILEI and APP-CTFs was also confirmed (Supplementary Fig. 8).

Recently, transforming growth factor-β (TGF-β) signalling in neuronal cells was reported to lead to decreased levels of APP-CTF and Aβ[31]. On the other hand, TGF-β selectively induces translation of ILEI via phosphorylation of heterogeneous nuclear ribonucleoprotein E1 in mammary gland cells[32]. Thus, we asked whether the inhibitory effect of TGF-β on Aβ production in brain is mediated by ILEI induction. To address this, we first examined ILEI induction and Aβ reduction by TGF-β using organotypic culture of rat forebrain slices. Next, we evaluated TGF-β-induced reduction in Aβ production from forebrain slices pretreated with ILEI-specific siRNA. TGF-β induced ILEI and reduced Aβ secretion, and these effects were almost completely abrogated in the ILEI-knockdown condition (Fig. 5b).

To evaluate the possible involvement of ILEI in AD pathogenesis, we examined the levels of secreted ILEI in autopsy brains of patients with sporadic AD. Soluble fractions from temporal cortex homogenates were subjected to immunoblotting. ILEI expression was normalized to the level of neuron-specific enolase in each sample to compensate for the difference in neuronal density. ILEI was significantly reduced in AD cases compared with age-matched non-neurological disease controls (Fig. 5c, $P=0.000$) and was inversely correlated with levels of Aβ or phosphorylated tau with semi-quantitative immunoblotting (Supplementary Fig. 9a,b). The ILEI level in autopsy brains with non-AD neurological diseases was equivalent to that of non-neurological disease control brains (Fig. 5c, $P=0.459$). Although our result is preliminary due to the limited number of cases examined, the trend is unequivocal. The decrease in ILEI did not seem to be secondary to brain Aβ accumulation, because ILEI is unaltered in the brains of aged APP-overexpressing mice[33] (Supplementary Fig. 9c).

ILEI ameliorates the phenotypes of AD model mice. To analyse the consequences of ILEI overexpression in mammalian brains, we developed Tg mice in which the mouse prion promoter was used to drive expression of a human ILEI cDNA transgene predominantly in the brain[34]. Heterozygous Tg mice exhibited normal development and fertility with no gross morphological defects. Similar to wild-type mice, ILEI expression was restricted to neuronal cells in the brains of Tg mice (Fig. 6a). Immunoblotting of brain homogenates indicated a three-fold increase in ILEI protein levels and no alteration in Notch intracellular domain levels in the Tg mice compared with non-Tg littermates (Fig. 6b). These findings suggest that the ILEI-Tg mice

Figure 4 | Secreted ILEI interacts with the PS1/γ-secretase complex and interferes with its APP-CTF-stabilizing property. (**a**) Effects of purified ILEI-VH (pILEI-VH) on Aβ secretion and cellular APP-CTFs. pILEI-VH was added to the culture medium of ILEI-knockdown HEK293 cells at the indicated concentrations (μg ml^{-1}). V5-His tag peptide (VH, 7 μg ml^{-1}) served as a negative control. Secreted Aβ40 was measured with ELISA assay and APP-CTFs were analysed with immunoblotting. The right graph shows the relative intensity of APP-CTFs normalized to β-actin ($n=3$, mean ± s.d.). (**b**) Laser scanning confocal microscopic images of pILEI-VH. pILEI-VH was immunostained with anti-V5 tag antibody (green) 0 or 4 h after its addition to the medium. Nuclei were stained with Hoechst 33342 (blue). Scale bar, 10 μm. (**c**) Co-immunoprecipitation assays for pILEI-VH and PS1. ILEI-knockdown HEK293 cells were lysed 0 or 4 h after addition of pILEI-VH, and the cell lysates were subjected to immunoprecipitation. A blot of the anti-ILEI precipitate was probed with anti-PS1-CTF or anti-V5 antibody. (**d**) ILEI-knockdown effects on APP-CTFs and secreted Aβ40 levels in PS1/PS2-knockdown, PEN-2-knockdown, or DAPT (*N*-[*N*-(3,5-difluorophenacetyl)-L-alanyl]-*S*-phenylglycine *t*-butyl ester; 1 μM)-treated HEK293 cells ($n=3$, mean ± s.d.). (**e**) Co-immunoprecipitation assays for PS1 and APP-CTFs. Cell lysates of native, ILEI-knockdown (k/d) and ILEI-overexpressing (oe) HEK293 cells were immunoprecipitated with anti-PS1 antibody (PS1-IP). (**f**) Co-immunoprecipitation assays for PS1 and ILEI. Cell lysates of native and Swedish APP-overexpressing (Sw-APP) HEK293 cells were immunoprecipitated with anti-PS1 antibody (PS1-IP). (**g**) Effects of PS1 mutants on ILEI function. Mock, D385A-PS1, CTm2-PS1 or TMD2m-PS1 was transfected into native, ILEI-knockdown (k/d) and ILEI-overexpressing (oe) HEK293 cells (the same cell lines as in **e**). The same amount of protein from cell membrane lysates was subjected to immunoblotting for APP-CTFs. α: APP-CTFα, β: APP-CTFβ. The graph shows the relative intensity of APP-CTFs normalized to native HEK293 cells transfected with the same plasmid ($n=3$, mean ± s.d.). For data from **a**, **d** and **g**, two-tailed Student's *t*-test was used to analyse statistical significance. $^{*}P<0.05$, $^{**}P<0.01$ and NS, not significant, versus control (**a**,**d**) or native (**g**).

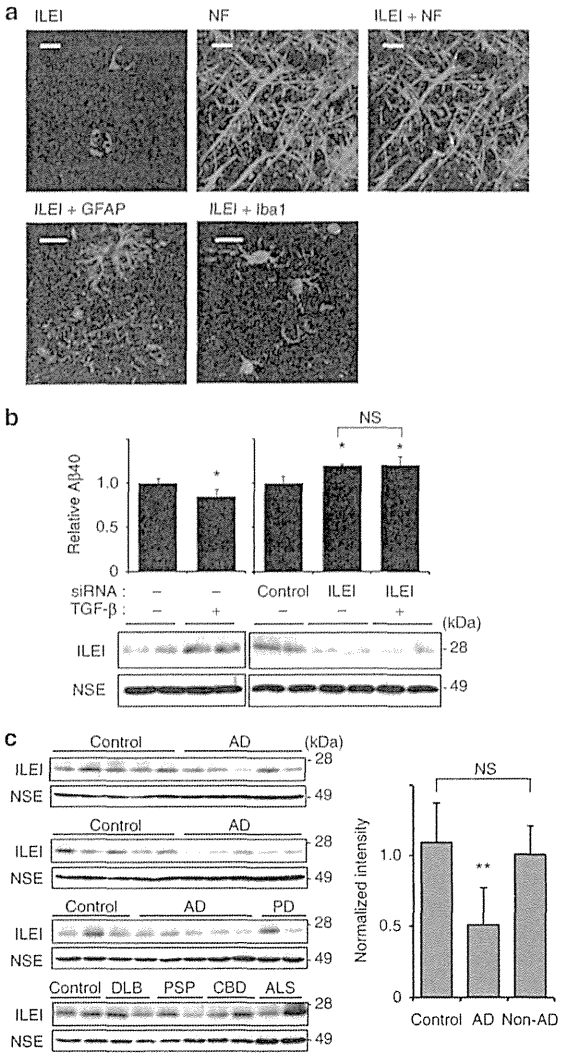

Figure 5 | Neuronal expression of ILEI is induced by TGF-β and reduced in AD brains. (**a**) Double immunostaining for ILEI and cell type-specific markers in mouse brain sections. Neurofilament (NF), glial fibrillary acidic protein (GFAP) and Iba-I are marker proteins for neurons, astrocytes and microglia, respectively. Scale bars, 10 μm. (**b**) Effects of TGF-β treatment on cultured rat brain slices pretreated with non-targeting control or ILEI-specific siRNA. Forebrain slices containing the hippocampus and cerebral cortex were prepared from three Wistar rats (3-week-old, female). The relative levels of Aβ40 ($n=3$, mean ± s.d.) and immunoblotting for ILEI are shown. Neuron-specific enolase (NSE) was used as a loading control. $^{*}P<0.05$ versus vehicle or control, and NS, not significant by Student's *t*-test. Aβ40 concentrations were as follows: control for TGF-β, 743.68 ± 39.32; TGF-β, 631.23 ± 54.36; control for ILEI-knockdown, 751.77 ± 60.23; ILEI-knockdown, 901.28 ± 12.61; ILEI-knockdown/TGF-β, 902.28 ± 72.57 pmol per g protein ($n=3$, mean ± s.d.). (**c**) Immunoblots for ILEI in Tris-buffered saline-extracted fractions from temporal cortices of AD patients ($n=15$, 82.0 ± 4.5 years old, post-mortem interval 7.0 ± 3.5 h), age-matched controls without neurological disease ($n=15$, 80.1 ± 1.7 years old, post-mortem interval 8.0 ± 5.4 h) and non-AD neurological disease controls ($n=10$, 79.6 ± 3.7 years old, post-mortem interval 9.3 ± 5.9 h). Non-AD disease controls were Parkinson's disease (PD), dementia with Lewy bodies (DLB), progressive supranuclear palsy (PSP), corticobasal degeneration (CBD) or amyotrophic lateral sclerosis (ALS). The graph shows the relative intensity of ILEI normalized to NSE (mean ± s.d.). $^{**}P<0.01$ versus control or non-AD control and NS, not significant by Student's *t*-test.

represent an appropriate model for ILEI overexpression without obvious ectopic expression. Immunoblotting revealed a 30% decrease in APP-CTFα and APP-CTFβ levels in the brains of Tg mice compared with controls (Fig. 6c), and the endogenous levels of Aβ40 and Aβ42 in Tris-buffered saline-soluble and -insoluble fractions of brain homogenates were significantly reduced in ILEI-Tg mice compared with non-Tg littermate controls (Fig. 6d). Thus, overexpression of ILEI suppresses APP-CTF accumulation and Aβ generation *in vivo* while sparing Notch processing.

To determine whether ILEI overexpression affects disease progression, we bred ILEI-Tg mice with Swedish mutant APP-overexpressing mice (APP-Tg, Tg2576), which show impaired learning and memory and brain Aβ deposition by 9–10 months of age[33]. APP/ILEI-double Tg mice appeared healthy and had a survival curve comparable with APP-Tg mice. We used a Y-maze test to assess hippocampus-dependent spatial working memory, which declines with age in APP-Tg mice[33]. At 11–13 months of age, but not at 6 months of age, APP-Tg mice showed poor performance ($n=12$, $P=0.0000$), but APP/ILEI-Tg mice showed similar performance ($n=11$, $P=0.3692$) compared with non-Tg littermate (Fig. 7a). We found no significant difference in locomotor activity or motivation to explore the maze (the total number of arm entries was 28.6 ± 3.75 in APP-Tg mice and 25.2 ± 4.08 in APP/ILEI-Tg mice; $P=0.5478$).

We next quantified the Aβ plaque load using brain sections immunohistochemically stained for Aβ. At 12 months of age, the plaque number and the area occupied by plaques in the cerebral cortex and hippocampus were clearly reduced in APP/ILEI-Tg mice compared with APP-Tg littermates (Fig. 7b–d). Moreover, quantitative analysis with Aβ enzyme-linked immunosorbent assay (ELISA) using brains of the same set of mice confirmed that the levels of Aβ40 and Aβ42 in soluble and insoluble fractions were significantly lower in APP/ILEI-Tg mice than in APP-Tg littermates (Fig. 7e,f). These results support the conclusion that ILEI efficiently reduces Aβ accumulation and ameliorates the memory deficit caused by Aβ overload in the brain.

Discussion

Our study shows that Aβ generation can be attenuated by overexpression or administration of ILEI. ILEI regulated Aβ generation by altering the stability of APP-CTFs by extracellular or luminal binding to the PS1/γ-secretase complex. ILEI exhibited functional selectivity for APP and did not affect Notch derivatives. Neuronal expression of ILEI was enhanced by TGF-β signalling in mammalian brain. The levels of secreted ILEI were reduced in autopsy brains of patients with sporadic AD. Tg overexpression of ILEI successfully ameliorated brain Aβ burden and memory deficits in AD model mice.

Based on a recent structural study showing that ILEI and pancreatic-derived factor (PANDER, also known as FAM3B) adopt a globular ββα fold that is distinct from the conformation of classical cytokines, the FAM3 superfamily members may represent a novel class of signalling molecules[35]. Earlier works have revealed that ILEI acts downstream of TGF-β to induce epithelial-to-mesenchymal transition of epithelial cells, whereas PANDER, which is cosecreted with insulin from pancreatic islet cells, is involved in regulation of insulin secretion and glycemic levels[28,36,37]. Expression of the ILEI transcript in human brain has been described[22]. However, the function of ILEI in the nervous system remains largely unknown, except for its possible role in development of the *Xenopus* retina[38]. Our results suggest that ILEI is induced by TGF-β also in mammalian brain. Multiple lines of evidence link TGF-β signalling to brain Aβ accumulation and development of AD[39]. Thus, the specific genotype + 10 C/C of the TGF-β1 gene, which affects the expression level of TGF-β1,

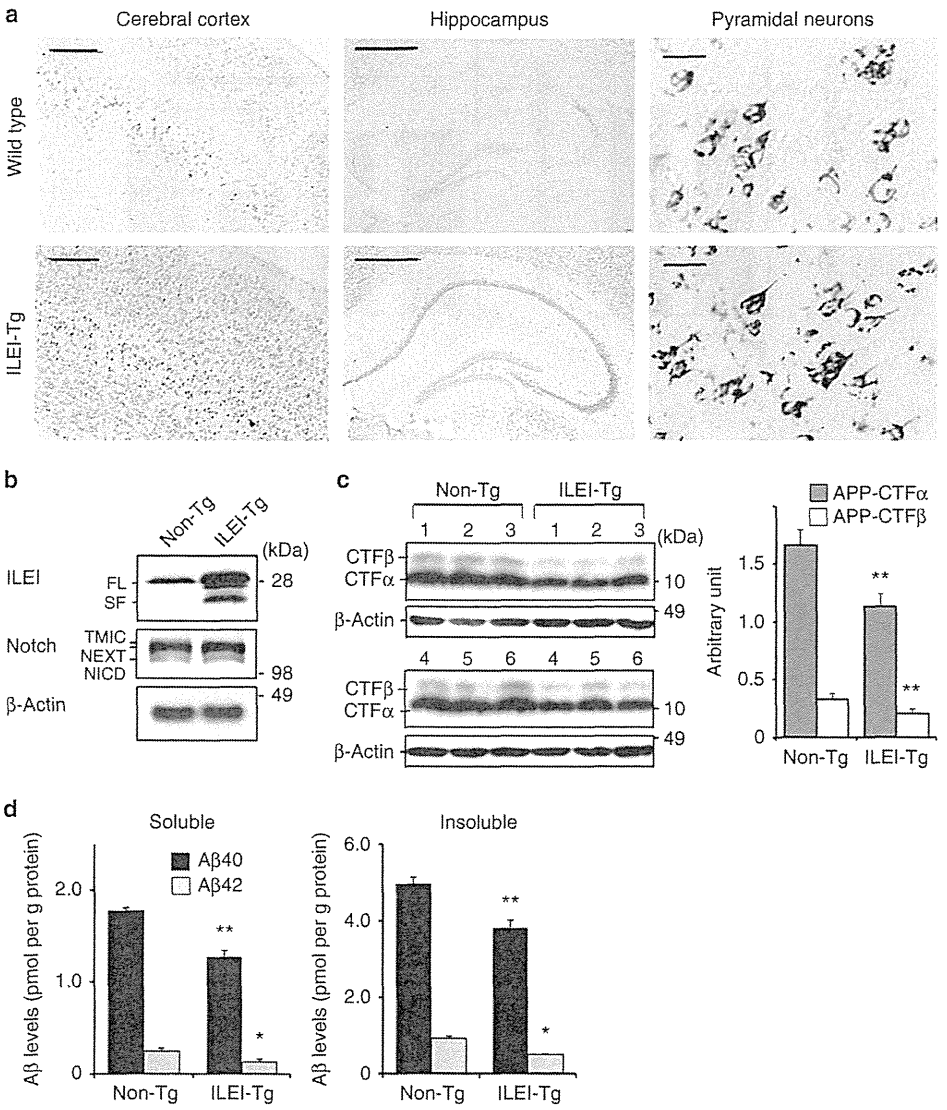

Figure 6 | The Aβ level is reduced in brains of ILEI-Tg mice. (**a**) Immunostaining shows ILEI expression in neurons of the cerebral cortex and hippocampus of wild-type and ILEI-Tg mouse brains (8 months old). Scale bars, 200 μm (left), 500 μm (centre), 20 μm (right). (**b**) Immunoblots for ILEI and Notch in brains of ILEI-Tg mice and non-Tg littermates (6 months old). β-Actin was used as a loading control. FL, full-length; SF, secreted form. (**c**) Immunoblots for APP-CTFs in brains of ILEI-Tg mice and non-Tg littermates (6–8 months old, $n=6$ per genotype). The graph shows the relative intensity of APP-CTFs normalized to β-actin ($n=6$, mean ± s.d.). $^{**}P<0.01$ versus non-Tg mice by Student's *t*-test. (**d**) Brain Aβ levels in non-Tg and ILEI-Tg mice (10 months old, $n=6$ per genotype). Aβ40 (black bars) and Aβ42 (grey bars) in Tris-buffered saline-soluble and -insoluble fractions of brain homogenates were measured using ELISA assays ($n=6$, mean ± s.d.). $^{*}P<0.05$ and $^{**}P<0.01$ versus non-Tg by Student's *t*-test.

is associated with an increased risk of AD[40], and the neuronal expression of TGF-β type II receptors is reduced in AD brains from the early stage of disease development[31]. In addition, recent proteomic analysis of cerebrospinal fluid revealed significantly decreased ILEI levels in patients with idiopathic temporal lobe epilepsy[41], in whom the age-related incidence of Aβ plaques in temporal cortex is significantly higher compared with age-matched controls[42]. The ILEI level in cerebrospinal fluid may also be a biomarker for AD[43]. These reports indirectly support our conclusion, indicating the functional relevance of ILEI to Aβ generation *in vivo* and the pathogenesis of AD.

A previous study using cultured neurons derived from APP-CTFβ-Tg mice indicated that 30% of APP-CTFβ is converted to Aβ[44]. APP-CTFs are also degraded through alternative pathways, including proteasomal, lysosomal and autophagosomal-lysosomal pathways[44–47]. In cultured neuronal cells, proteasome inhibition increases Aβ generation by augmenting the amount of APP-CTFβ[44,45]. Hence, ILEI knockdown may increase Aβ generation by inhibiting APP-CTFβ degradation through pathways that do not lead to Aβ production. Alteration of APP-CTF stability by ILEI required cellular expression of the γ-secretase complex, regardless of whether the complex was enzymatically active or inactive. A large pool of the PS1/γ-secretase complexes remains catalytically inactive in the cell[48]. Even active γ-secretase complexes stably bind to APP-CTFs on substrate-docking sites, which are spatially separated from the catalytic centre[21,49].

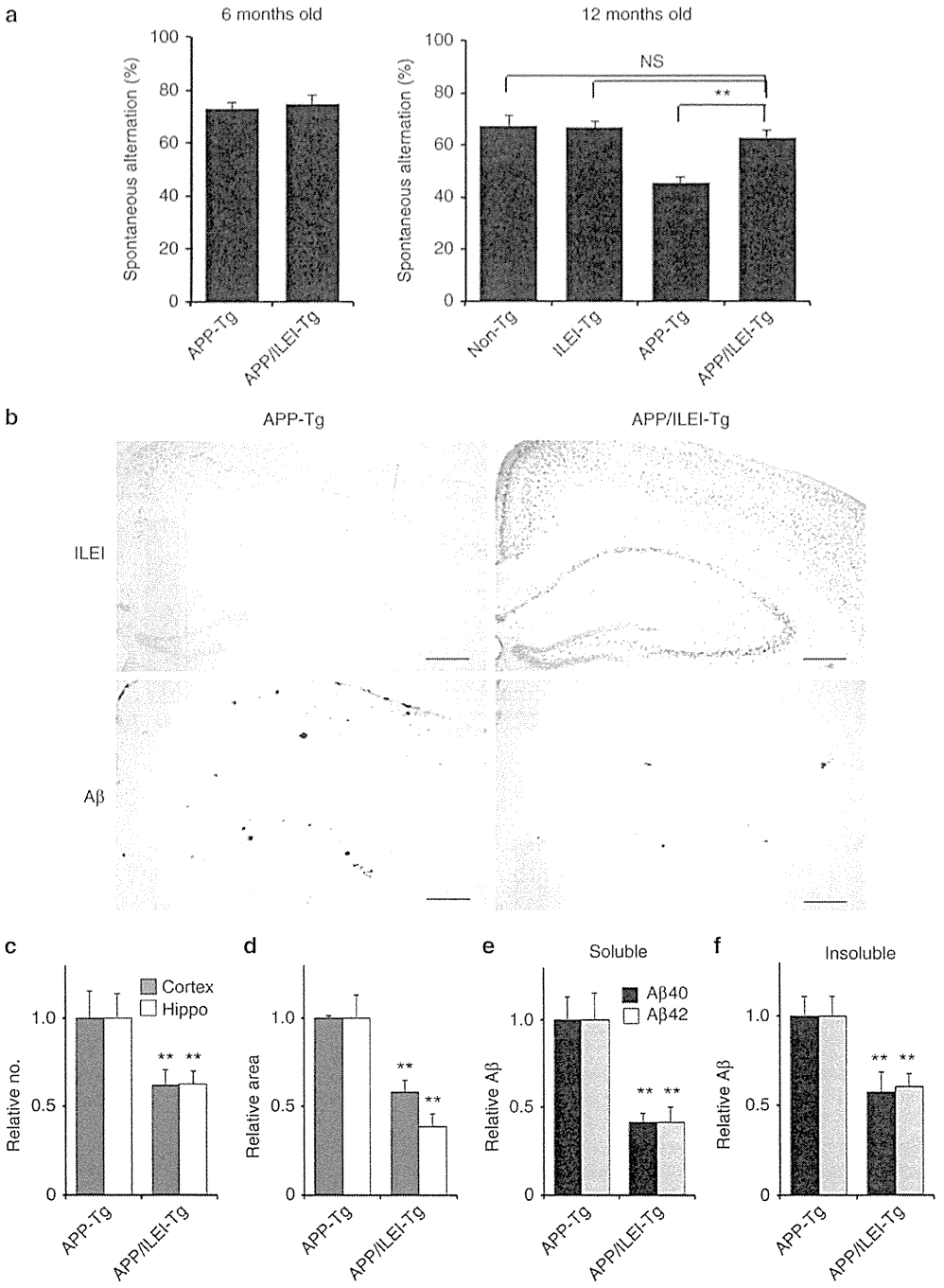

Figure 7 | ILEI overexpression ameliorates the memory deficit and reduces brain Aβ burden in APP-Tg mice. (**a**) Spontaneous alternation in the Y-maze test. APP-Tg (3 females at 6 months age, 6 males and 6 females at 12 months age), ILEI-Tg (5 males and 4 females at 12 months age), APP/ILEI-Tg (3 females at 6 months age, 5 males and 6 females at 12 months age) and non-Tg (5 males and 4 females at 12 months age) littermate mice were used. Data are expressed as percentage (mean ± s.e.m.). $^{**}P<0.01$, NS, not significant by Student's *t*-test. (**b**) Immunostaining images with anti-ILEI antibody (top) and anti-Aβ antibody (bottom) using serial brain sections from 12-month-old APP-Tg (left) and APP/ILEI-Tg (right) mice. Scale bars, 200 μm. (**c**–**f**) Aβ burden in brains of APP-Tg and APP/ILEI-Tg mice (12 months old, $n=6$ per genotype). The plaque number (**c**) and the area occupied by plaques (**d**) in Aβ-immunostained sections of prefrontal cortex (grey bars) and hippocampus (white bars) (mean ± s.e.m.). The relative levels of Aβ40 (black bars) and Aβ42 (grey bars) in soluble (**e**) and insoluble (**f**) fractions (mean ± s.e.m.). $^{**}P<0.01$ versus the APP-Tg by Student's *t*-test. Aβ concentrations were as follows: soluble Aβ40 of APP-Tg, 19.79 ± 2.66; soluble Aβ42 of APP-Tg, 4.69 ± 0.72; insoluble Aβ40 of APP-Tg, 1362.56 ± 152.88; insoluble Aβ42 of APP-Tg, 517.80 ± 57.82; soluble Aβ40 of APP/ILEI-Tg, 8.14 ± 1.21; soluble Aβ42 of APP/ILEI-Tg, 1.95 ± 0.42; insoluble Aβ40 of APP/ILEI-Tg, 788.68 ± 142.23; insoluble Aβ42 of APP/ILEI-Tg, 312.92 ± 38.80 pmol per g protein (mean ± s.e.m.).

Enhanced expression of PS1 in cultured insect and mammalian cells increases the accumulated level of APP-CTFβ by extending its half-life independent of γ-secretase activity[25]. Thus, the PS1/γ-secretase complex also functions as a chaperone that protects APP-CTFs from nonspecific degradation. Chaperone properties of the γ-secretase complex have been described only for APP but not for other substrates. Our results indicate that ILEI inhibits this stabilizing ability by directly binding to PS1-CTF without inhibiting γ-secretase activity, resulting in decreased accumulation of APP-CTFs and diminished generation of Aβ. This possibility is supported by the finding that ILEI is localized in the *trans*-Golgi network and the endocytic vesicles where PS1:CTFβ complexes are located and Aβ is produced[29,30].

Several proteins regulate the stability of APP by directly binding or phosphorylating its cytoplasmic domain[50]. In contrast, ILEI selectively accelerated γ-secretase-independent degradation of APP-CTFs through a novel mechanism in which ILEI interacted with the PS1/γ-secretase complex but not APP on the extracellular or luminal side of the membrane. Modifier of cell adhesion, which is known as dedicator of cytokinesis 3, a member of the dedicator of cytokinesis family of guanine nucleotide exchange factors, binds presenilins and selectively accelerates proteasome-mediated degradation of APP[51]. However, in contrast to ILEI, modifier of cell adhesion is a cytoplasmic protein that binds to presenilins on the cytoplasmic side of the membrane and destabilizes both APP-FL and APP-CTFs via an unknown mechanism[52]. Conversely, platelet-activating factor acetylhydrolase, isoform 1b, subunit 2 and sphingolipids inhibit γ-secretase-independent degradation of APP-CTFs and increase Aβ production[53,54].

Previous studies have revealed a significant increase in APP-CTFβ as well as Aβ in sporadic AD brains, which is sometimes associated with hyperactivity of β-secretase/BACE1 or downregulation of TGF-β signalling[5,6,31]. In addition, the protein degradation activities of proteasomes, lysosomes and autophagy gradually decline with age and contribute to high levels of APP-CTFβ and Aβ, and consequently to an increased risk of sporadic AD[7,8,45]. On the other hand, clinical trials using non-selective inhibitors of γ-secretase activity were discontinued due to adverse effects that were probably caused by Notch inhibition and APP-CTF accumulation[11–13,55]. Thus, ILEI may be a plausible target for the development of disease-modifying therapies for AD, because ILEI may alter disease progression without perturbing Notch signalling and increasing APP-CTFβ.

Methods

Plasmids. For construction of srPEN-2 (ref. 24), three silent nucleotide substitutions were introduced into human PEN-2 cDNA by PCR-based site-directed mutagenesis using the primer: 5′-GAACAGAGCCAAATCAAAGGTTACGTAT GGCGCTCAGCTGTGGGCTTCCTCTTC-3′. The pcDNA3-TAP plasmid containing DNA for the TAP tag, which consists of two immunoglobulin-binding domains of protein A from *Staphylococcus aureus*, a cleavage site for the tobacco etch virus (TEV) protease and the calmodulin-binding polypeptide, was obtained from Dr K. Oshikawa (Kyushu Universiy, Fukuoka, Japan). To generate pTAP-srPEN-2, the TAP tag fragment was fused in-frame to the 5′-end of srPEN-2 cDNA in pcDNA4 (Invitrogen, Carlsbad, CA, USA). A cDNA encoding ILEI with or without the stop codon was amplified from a human brain cDNA library (Clontech, San Diego, CA, USA) using PCR and was then ligated into pcDNA6/V5-His (Invitrogen). To construct the ILEI knockdown vector, the oligonucleotide 5′-GGAGAAGUAUUAGACACU-3′ was ligated into pSUP (Oligoengine, Seattle, WA, USA). To prepare an expression plasmid for siRNA-resistant ILEI, five neutral mutations were introduced into ILEI cDNA by PCR-based site-directed mutagenesis using the primer: 5′-GAAAAACAGGAGAGGTTCTGGATACTAA ATATTTTG-3′. The expression plasmids for PS1 mutants were constructed by PCR-based mutagenesis using the expression plasmid for wild-type human PS1 (ref. 56) as template. The sequences of all constructs were confirmed by sequencing. NotchΔE[57] and HES-Y[58] are gifts from Drs Raphael Kopan (Washington University, St Louis, MO, USA) and Masayasu Okochi (Osaka University, Osaka, Japan), respectively.

Identification of ILEI. To generate the HEK-TAP-PEN-2 and HEK-TAP empty cell lines, we transfected HEK293 cells (CRL-1573, ATCC) stably expressing PEN-2-specific siRNA with pTAP-srPEN-2 or pTAP-empty. HEK-TAP-PEN-2 or HEK-TAP-empty cells were homogenized in buffer A (20 mM Tris (pH 7.5), 150 mM NaCl, 0.5 mM EDTA) containing a protease inhibitor cocktail (Roche Diagnostics, Mannheim, Germany). The postnuclear supernatants were centrifuged at 100,000 *g* for 1 h to collect the microsome membrane pellets. The pellet was solubilized in buffer A containing 1% CHAPSO and then mixed with IgG-sepharose beads followed by incubation at 4 °C for 2 h. The mixture was washed with buffer A containing 0.5% CHAPSO. The beads were incubated with 10 U of TEV protease in TEV buffer (10 mM Tris (pH 8.0), 150 mM NaCl, 0.5 mM EDTA, 0.5% CHAPSO) at 4 °C for 12 h. After adjustment of the calcium concentration to 200 μM, the supernatant was mixed with calmodulin resin in three volumes of buffer B (10 mM Tris (pH 8.0), 150 mM NaCl, 1 mM Mg acetate, 1 mM imidazol, 2 mM $CaCl_2$, 0.5% CHAPSO) and then incubated for 5 h at 4 °C. The proteins were eluted with SDS sample buffer and subjected to SDS–PAGE. The gel was stained with silver or SYPRO Ruby (Molecular Probes, Eugene, OR, USA). Bands were excised from the gel, and proteins in each gel piece that contained a specific band or a group of specific bands were digested with trypsin and subjected to liquid chromatography-tandem mass spectrometry followed by a search of the Mascot database.

Immunoblotting analysis. The same amount of protein from cell lysates was loaded onto SDS–PAGE and transferred to a polyvinylidene fluoride membrane (Millipore, Billerica, MA, USA) or nitrocellurose membrane (BioRad, Hercules, CA, USA). The membranes were incubated with the following primary antibodies at 4 °C overnight, washed and incubated with corresponding horseradish peroxidase-conjugated secondary antibodies (1:3,500, Invitrogen) for 1 h. Anti-human ILEI polyclonal antibody was raised in rabbits against a thyroglobulin-conjugated synthetic polypeptide corresponding to amino acid residues 126 to 143 with an added amino-terminal Cys residue (C + GGDVAPFIEFLKAIQDGT). This antibody was purified using immunoaffinity chromatography with immobilized antigen (1:4,000). The following antibodies were also used: goat polyclonal anti-FAM3C antibody (1:2,000, R&D Systems, Minneapolis, MN, USA); rabbit polyclonal anti-NCT (1:5,000), anti-APP-CTF (1:10,000) and mouse monoclonal anti-β-actin (1:10,000) antibodies (Sigma, St Louis, MO, USA); mouse monoclonal anti-PS1 loop antibody (1:3,500, Chemicon, Temecula, CA, USA); rabbit polyclonal anti-APH-1L antibody (1:2,000, Covance, Princeton, NJ, USA); rabbit polyclonal anti-PEN-2 antibody (1:2,000, Calbiochem, San Diego, CA, USA); mouse monoclonal anti-Notch-1 antibody (mN1A, 1:1,000, AbD Serotec, Kidlington, UK); rabbit monoclonal anti-LRP1 antibody (1:5,000, Abcam, Cambridge, MA, USA); rabbit polyclonal anti-cadherin antibody (1:10,000, Sigma); mouse monoclonal antibody specific for the 17–26 amino acid residues of the human Aβ (4G8, 1:1,000, Covance); rabbit polyclonal anti-neuron-specific enolase (1:10,000, Assay Biotechnology, Sunnyvale, CA, USA). Original immunoblots can be found in Supplementary Fig. 10.

Co-immunoprecipitation and chemical crosslinking. Cultured cells were lysed in a lysis buffer containing 1% CHAPSO. After pre-clearing with protein G-Sepharose 4 fast flow (GE Healthcare, Tokyo, Japan) for 1 h, postnuclear supernatants were incubated with the appropriate antibody. The immunoprecipitates were recovered by overnight incubation with protein G-Sepharose and were analysed with immunoblotting. To eliminate IgG light-chain bands on immunoblots, signals were detected with horseradish peroxidase-conjugated bio-nanocapsules incorporating IgG Fc-binding *Z* domains derived from *S. aureus* protein A[59] (Beacle, Kyoto, Japan) instead of the secondary antibody. For crosslinking, HEK293 cells were treated with 2 mM dithiobis succinimidyl propionate (Thermo Fisher Scientific, Kanagawa, Japan) for 2 h on ice. The reaction was stopped by adding Tris–HCl (pH 7.5, final 20 mM). After incubating on ice for 15 min, the cells were lysed with a lysis buffer containing 1% Nonidet P-40. Under this condition, non-crosslinked components of the γ-secretase complex were reduced by >80% on immunoblotting. After centrifugation at 12,000g, the supernatant was subjected to co-immunoprecipitation.

RNA interference. The following siRNA duplexes were purchased from Dharmacon (Lafayette, CO, USA): siGENOME SMART pool M-020514 for ILEI and D001210 for a non-targeting control. The M-020514 pool consisted of the four duplexes targeting the following sequences; F1: 5′-GAACAGCACAUAAAGAA CA-3′; F2: 5′-GGAGAAGUAUUAGACACUA-3′; F3: 5′-GGAGCACAUCUA UUACUAA-3′; F4: 5′-GAACAAUAAGGAUACAAAC-3′. Cultured cells were transfected with individual or pooled siRNA duplexes using Lipofectamine RNAi MAX (Invitrogen).

Secretase activity assays. For a cell-free γ-secretase assay, cultured cells were homogenized in HEPES buffer (25 mM HEPES (pH 7.0), 150 mM NaCl, 5 mM $MgCl_2$, 5 mM $CaCl_2$, a protease inhibitor cocktail) and the postnuclear supernatants were centrifuged at 100,000 *g* for 1 h. The membrane pellets were lysed in 1% CHAPSO/HEPES buffer. Solubilized γ-secretase was recovered by centrifugation at 100,000 *g* for 30 min, and the concentrations of protein and CHAPSO were adjusted to 0.25 mg ml^{-1} and 0.25%, respectively. The resulting